CSIAM Trans. Appl. Math.
doi: 10.4208/csiam-am.SO-2025-0016

Vol. **x**, No. x, pp. 1-31
xx 2025

Exploring Fractional-Order Nonlinear Dynamics in Biodiesel Production with Optimal Control

Sk Mosaraf Ahammed[1], Oluwole Daniel Makinde[2], Tushar Ghosh[1] and Priti Kumar Roy[1,*]

[1] *Center of Mathematical Biology and Ecology, Department of Mathematics, Jadavpur University, West Bengal, Kolkata-700032, India.*
[2] *Faculty of Military Science, Stellenbosch University, Private Bag X2, Saldanha 7395, South Africa.*

Received 24 Febuary 2025; Accepted 28 April 2025

Abstract. Biodiesel, a sustainable and renewable energy source, is a promising alternative to fossil fuels. The transesterification process of biodiesel production effectively captures memory effects in reaction kinetics. In this study, we developed two fractional order models of the chemical catalytic transesterification reaction to explore the memory effects of the reaction kinetics utilizing two different non-singular kernel methods: Caputo-Fabrizio and Atangana-Baleanu in the Caputo sense. We compared the results with experimental data of biodiesel production and demonstrated the existence and uniqueness of the solution for the fractional system. A sensitivity analysis is performed using the Latin hypercube sampling method to evaluate the impact of various parameters on biodiesel production, followed by the computation of partial rank correlation coefficients based on Pearson's correlation coefficient. We exhibit the dynamic behavior of all reactants corresponding to these fractional models with the variation of fractional order and the memory rate parameter. Additionally, we display the memory effect through the surface plots for biodiesel production by varying fractional order, molar ratio, and ultrasound frequency. Our numerical comparison with experimental data identifies the fractional-order value for the best fit of biodiesel production and can be increased by applying optimal control on ultrasound frequency.

AMS subject classifications: 34A08, 49-XX

Key words: Waste cooking oil, biodiesel, optimal control, Caputo-Fabrizio operator, Atangana-Baleanu in Caputo sense.

1 Introduction

Biodiesel is a leading alternative energy source to replace fossil fuels due to its favorable properties. It can be produced from various sources like vegetable oils, animal fats, mi-

*Corresponding author. *Email address:* pritiju@gmail.com (P. K. Roy)

croorganisms, or waste cooking oil using a transesterification reaction catalyzed by either a base or an enzyme. Jatropha curcas and waste cooking oil are ideal for biodiesel production because they are non-food sources, reducing competition with food crops, and are cost-effective, with Jatropha thriving on marginal land and waste oil utilizing discarded resources. Waste cooking oil (WCO) is a by-product of various cooking processes in households, restaurants, food industries, and catering services. Improper disposal of waste cooking oil harms the environment by clogging drains, polluting water bodies, and releasing methane from landfills, contributing to climate change [11]. Reusing degraded oil in some food industries can increase harmful carcinogens like acrylamide and polycyclic aromatic hydrocarbons (PAHs), posing health risks such as cancer and cardiovascular diseases [13]. Despite its environmental and health concerns, waste cooking oil holds significant potential for sustainable applications. One of the most prominent uses of WCO is in the production of biodiesel, a renewable, eco-friendly alternative to fossil fuels [4, 21]. Biodiesel production from waste cooking oil contributes to a circular economy, where waste is turned into valuable products, ensuring sustainability and reducing overall waste generation [16]. It consists of triglycerides, but it often contains impurities such as water, free fatty acids (FFAs), food particles, and other organic matter. The transformation process primarily involves cleaning and preparing the oil for the transesterification reaction (see Fig. 1), which converts triglycerides into biodiesel [6].

Fractional-order derivatives have gained significant attention in mathematical modeling due to their ability to capture memory effects and hereditary properties in com-

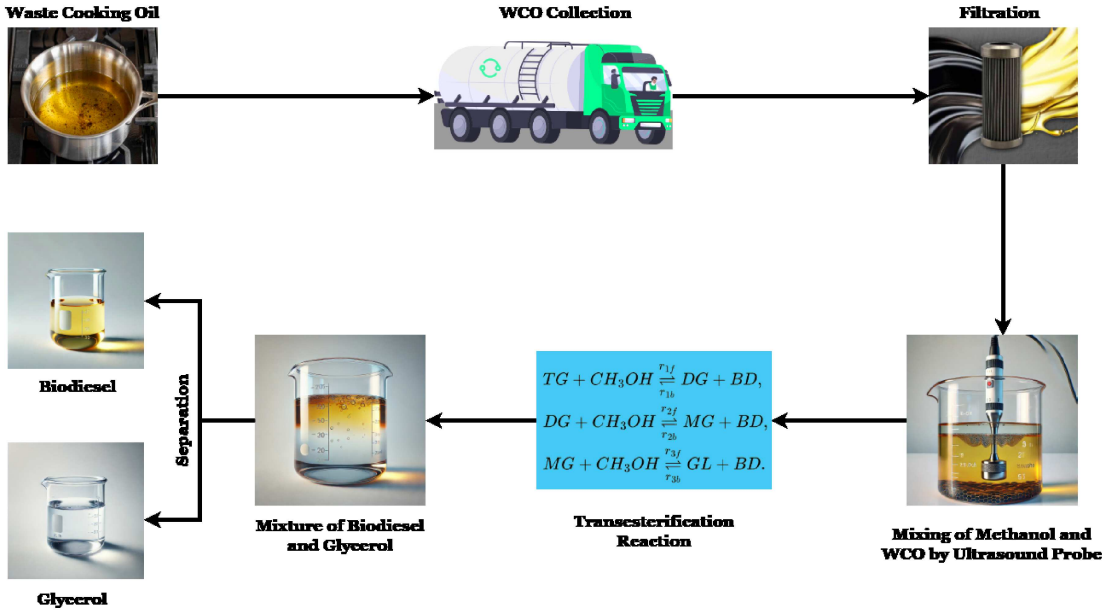

Figure 1: Scheme for WCO collection from various restaurants and households, filtration and transesterification reaction to produce biodiesel using ultrasound frequency.

plex systems. Unlike classical integer-order derivatives, fractional derivatives provide a more generalized approach to describing dynamical processes where past states influence the present behavior [17]. This memory effect arises from the integral representation of fractional derivatives, where the function's past values contribute to its current rate of change. This feature makes fractional derivatives highly effective in modeling real-world phenomena, such as viscoelasticity, diffusion processes, and reaction kinetics. Several fractional derivative formulations exist, each defined by different kernel functions that characterize the memory influence [23]. Among these, the Caputo-Fabrizio (CF) and Atangana-Baleanu in the Caputo sense (ABC) fractional operators have been widely studied due to their unique non-singular kernel structures. The Caputo-Fabrizio fractional derivative is characterized by a non-singular exponential kernel, which provides a smooth memory effect without singularities [9]. This property makes it suitable for modeling systems where past states influence current dynamics in a balanced manner. On the other hand, the Atangana-Baleanu fractional derivative employs a Mittag-Leffler function as its kernel, offering a more generalized memory representation that bridges classical fractional and integer-order derivatives [3]. This non-local and non-singular kernel allows for a more flexible modeling of memory effects in complex systems. These formulations have been extensively applied in modeling diffusion, reaction-diffusion systems, and complex dynamical processes, where the choice of kernel significantly affects the accuracy and stability of the model.

Khan *et al.* [14] performed a comparative analysis of heat and mass transfer in second-grade fluids over a vertical plate, employing both Caputo-Fabrizio and Atangana-Baleanu fractional derivatives. The study revealed that the Atangana-Baleanu derivative predicts a faster fluid flow compared to the Caputo-Fabrizio derivative, highlighting the influence of the chosen fractional operator on the dynamics of heat and mass transfer processes. Singh *et al.* [20] investigated a chemical kinetics system utilizing the Atangana-Baleanu derivative. Their study concluded that the Atangana-Baleanu derivative offers a more robust framework for modeling chemical kinetics, effectively capturing the complex memory effects inherent in such systems. Sheikh *et al.* [19] investigated the free convection flow of a generalized Casson fluid, considering heat generation and a first-order chemical reaction, using both Atangana-Baleanu and Caputo-Fabrizio fractional derivatives. Their results showed that, at unit time, both fractional derivatives yield identical velocity predictions. The study by Edessa [10], indicates that the Caputo-Fabrizio derivative offers a more precise depiction of enzyme kinetics compared to traditional integer-order approaches.

Biodiesel production processes, such as transesterification, can exhibit memory effects where the current state depends not only on the present conditions but also on past states. The memory phenomenon in biodiesel kinetics represents the influence of past reaction states on the current rate of transesterification, capturing the hereditary effects of reactant interactions and catalyst efficiency over time. Physically, this means that the reaction does not instantaneously respond to changes in conditions but instead retains a cumulative effect, leading to a more gradual and controlled conversion of triglycerides

into biodiesel, which can enhance process stability and yield optimization. Fractional-order derivatives naturally incorporate these memory effects, making them suitable for capturing the dynamics of such processes. In biodiesel production, reaction kinetics can be complex and involve multiple steps with varying rates. Fractional-order models can provide a more flexible and accurate description of these kinetics compared to classical integer-order models. In the literature, only one research article has been published on biodiesel production using fractional-order derivatives. Basir *et al.* [2] applied fractional-order modeling to enzymatic biodiesel synthesis, utilizing mechanical stirring to ensure proper mixing of the reactants. Their study demonstrated that the presence of memory effects in the process led to increased biodiesel production when using a fractional order of 0.9, compared to models based on an integer-order derivative. From this study, questions may arise regarding whether base-catalyzed transesterification exhibits memory effects in biodiesel production. If so, which method between CF and ABC provides a more accurate description of the memory effect for the dynamics of biodiesel production?

In this study, we investigate the impact of memory effects on biodiesel production by developing two fractional-order models using the CF and ABC fractional operators to describe the transesterification reaction WCO. The existence and uniqueness of the ABC model are established using the Banach fixed-point and Arzelà-Ascoli theorems. To assess the influence of key parameters on biodiesel yield, we conduct a sensitivity analysis utilizing Latin hypercube sampling (LHS) and partial rank correlation coefficients (PRCC). Analytical and numerical solution schemes are formulated to capture the memory effects, and comparative as well as surface plots are presented to illustrate variations in biodiesel production under different conditions. The models are validated against experimental data for both CF and ABC operators. Additionally, an optimal control strategy for ultrasound frequency is derived using the ABC method to enhance biodiesel production, and its effectiveness is numerically demonstrated.

2 Preliminaries

Definition 2.1 ([8]). *The Caputo fractional derivative of order $\alpha\in(n-1,n]$ of $f(x)$ is defined as*

$$ {}^{C}_{a}D^{\alpha}_{x}f(x)=\frac{1}{\Gamma(\mathrm{n}-\alpha)}\int_{a}^{x}(x-t)^{n-\alpha-1}f^{n}(t)dt,\quad n=[\alpha]+1. $$

Definition 2.2 ([9]). *Let $f\in\mathcal{H}'(a,b), b>a, 0<\phi<1$. Then, the CF fractional differential operator is defined as follows:*

$$ {}^{CF}D^{\phi}_{x}(f(x))=\frac{M(\phi)}{1-\phi}\int_{0}^{x}\exp\left[-\frac{\phi(x-t)}{1-\phi}\right]f'(t)dt,\quad x\geq 0,\quad 0<\phi<1. $$

The function $M(\phi)$ serves as a normalization function, dependent on ϕ and meets the condition $M(0)=M(1)=1$.

Definition 2.3 ([3]). *The ABC fractional derivative in Caputo sense of a function $f(x)\in\mathcal{H}^1(a,b)$, $b>a$ with $\theta\in(0,1]$ is defined as*

$$ {}^{ABC}_{a}D^{\theta}_{x}f(x)=\frac{\vartheta(\theta)}{1-\theta}\int_a^x \frac{\mathrm{d}f}{\mathrm{d}t}E_\theta\left[-\frac{\theta}{1-\theta}(x-t)^\theta\right]\mathrm{d}t,$$

where $\mathcal{H}^1(a,b), b>a$ is a space of square-integrable functions and is defined as

$$\mathcal{H}^1(a,b)=\{f(x)\in\mathbb{L}^2(a,b)\mid f'(x)\in\mathbb{L}^2(a,b)\},$$

and $\vartheta(\theta)=1-\theta+\theta/\Gamma(\theta)$.

Definition 2.4 ([3]). *Let $f\in H^1(a,b)$ and $\theta\in(0,1]$. The θ-th ABC fractional integral of the function $f(x)$ is*

$$ {}^{AB}_{a}\mathrm{I}^{\theta}_{x}f(x)=\frac{(1-\theta)}{\vartheta(\theta)}f(x)+\frac{\theta}{\vartheta(\theta)\Gamma(\theta)}\int_a^x\frac{f(s)}{(x-s)^{1-\theta}}ds,\quad x\in[a,b],$$

where $\vartheta(\theta)$ is as defined in above.

3 The basic integer-order model and the corresponding CF and ABC fractional order model formulation

To develop a mathematical model for the transesterification reaction between waste cooking oil (triglycerides) and methanol for biodiesel production, the following key assumptions are considered:

- [L1]: The transesterification process consists of three consecutive and reversible reaction steps, where triglycerides react with methanol to produce biodiesel and glycerol as a byproduct [12].
- [L2]: The reaction mixture contains a minimal amount of water (0.2% w/w), which is insufficient to significantly influence hydrolysis reactions. Hence, hydrolysis is neglected in this model [24].
- [L3]: Since free fatty acids (FFAs) and other impurities are removed before transesterification, the saponification reaction is assumed to be negligible.

In transesterification, mass transfer resistance at the interface between methanol and triglyceride phases plays a crucial role, particularly in heterogeneous reaction systems where the reactants are immiscible. Factors such as high viscosity, poor solubility, and

diffusion limitations contribute to mass transfer resistance. Ultrasound application significantly improves mass transfer by reducing phase boundary resistance through cavitation, leading to enhanced diffusion. The mass transfer coefficient, considering ultrasound effects, is estimated using a modified Dittus-Boelter correlation [7]

$$M_c = \frac{1}{M_r} = 0.023\frac{D}{d^2}(Re)^{0.8}(Sc)^{0.33} = 0.023\frac{D}{d^2}\left(\frac{d^2\rho H}{\mu}\right)^{0.8}\left(\frac{\mu}{\rho D}\right)^{0.33}, \tag{3.1}$$

where M_r represents mass transfer resistance (inverse of the mass transfer rate), while R_e and Sc denote the Reynolds and Schmidt numbers, respectively. The parameters D, ρ, μ correspond to diffusivity, density, and viscosity of waste cooking oil, while d is the reactor vessel diameter, and H is the applied ultrasound frequency. Based on our previous studies [7] and [1], we identified that the optimal conditions for biodiesel production using ultrasound frequency are $H = 50$kHz, $T = 50^\circ$C, a methanol-to-triglyceride molar ratio is $5:1$, and a reactor diameter $d = 1$ meter. This whole study is conducted under these optimized conditions.

The transesterification reaction occurs in the presence of a potassium hydroxide catalyst and follows a three-step reversible mechanism [12]:

Step 1: Triglyceride (TG) reacts with methanol (AL) to form diglyceride (DG) and biodiesel (BD).

Step 2: Diglyceride reacts with methanol to produce monoglyceride (MG) and biodiesel.

Step 3: Monoglyceride reacts with methanol to yield biodiesel and glycerol (GL).

The overall reaction is

$$\begin{aligned} TG + CH_3OH &\underset{r_{1b}}{\overset{r_{1f}}{\rightleftharpoons}} DG + BD, \\ DG + CH_3OH &\underset{r_{2b}}{\overset{r_{2f}}{\rightleftharpoons}} MG + BD, \\ MG + CH_3OH &\underset{r_{3b}}{\overset{r_{3f}}{\rightleftharpoons}} GL + BD. \end{aligned} \tag{3.2}$$

The rate constants r_{1f}, r_{2f}, r_{3f} (forward reaction) and r_{1b}, r_{2b}, r_{3b} (backward reaction) follow the Arrhenius equation

$$r_i = A_i e^{\frac{-E_{A_i}}{RT}}, \tag{3.3}$$

where A_i is the frequency factor, E_{A_i} is the activation energy, T is the reaction temperature, and R is the universal gas constant [5]. Here in Table 1 reaction rates of the transesterification reaction are given and in Table 2 other parameter values used in the formation of mass transfer coefficient are given.

Table 1: Values of various reaction rate constants used in the transesterification reaction, adopted from [22]. These constants are essential for modeling the biodiesel production process and influence the reaction kinetics.

Parameter	Definition	Value ($\text{mole}^{-1}\text{Lmin}^{-1}$)
r_{1f}	Forward reaction constant	0.102
r_{1b}	Backward reaction constant	0.021
r_{2f}	Forward reaction constant	0.053
r_{2b}	Backward reaction constant	0.010
r_{3f}	Forward reaction constant	0.015
r_{3b}	Backward reaction constant	0.164

Table 2: Some liquid properties of waste cooking oil and input range of ultrasound and vessel size used in the reaction at 50° C.

Parameter	Definition	Value
D	Diffusivity of WCO	1.00×10^{-7}-$1.5\times10^{-7}\,\text{m}^2\cdot\text{s}^{-1}$
ρ	Density of WCO	$880\,\text{kg}\cdot\text{m}^{-3}$
μ	Viscosity of WCO	$26.1\,\text{kg}\cdot\text{m}^{-1}\cdot\text{s}^{-1}$
d	Vessel diameter	1 m
H	Ultrasound frequency	30-60 kHz

3.1 Integer-order differential system

The governing ordinary differential equations (ODEs) for the reaction mechanism, considering mass transfer effects, are formulated as follows:

$$\begin{cases} \dfrac{dT}{dt} = -r_{1f}TA + r_{1b}DB, \\ \dfrac{dA}{dt} = -r_{1f}TA + r_{1b}DB - r_{2f}DA + r_{2b}MB - r_{3f}MA + r_{3b}GB, \\ \dfrac{dD}{dt} = r_{1f}TA - r_{1b}DB - r_{2f}DA + r_{2b}MB, \\ \dfrac{dM}{dt} = r_{2f}DA - r_{2b}MB - r_{3f}MA + r_{3b}GB, \\ \dfrac{dB}{dt} = r_{1f}TA - r_{1b}DB + r_{2f}DA - r_{2b}MB + r_{3f}MA - r_{3b}GB + \dfrac{B}{M_r}\left(1 - \dfrac{B}{B_{\max}}\right), \\ \dfrac{dG}{dt} = r_{3f}MA - r_{3b}GB, \end{cases} \tag{3.4}$$

where T, A, D, M, B and G are the concentration of triglyceride, methanol, diglyceride, monoglyceride, biodiesel, and glycerol, respectively with initial condition $T(0) = T_0$, $A(0) = A_0, D(0) = 0, M(0) = 0, B(0) = 0$ and $G(0) = 0$.

Now, we extend the integer-order model to a fractional-order framework by replacing the time derivative with two distinct non-singular kernels: the exponentially decay type

kernel and the Mittag-Leffler kernel. However, this substitution disrupts dimensional consistency, as directly replacing an integer-order derivative with a fractional derivative (CF or ABC) in a dimensionally balanced equation is mathematically still questionable. To resolve this issue, we introduce the memory rate parameter R with dimensions as same as (1/minute) on the left side of the fractional model. This memory rate parameter ensures dimensional coherence, preserving mathematical consistency and stability in the modified system.

3.2 Caputo-Fabrizio fractional model

Using the CF fractional operator, the model is reformulated as

$$\begin{cases} R^{(1-\phi)\ CF}D_t^{\phi}T(t) = -r_{1f}TA + r_{1b}DB, \\ R^{(1-\phi)\ CF}D_t^{\phi}A(t) = -r_{1f}TA + r_{1b}DB - r_{2f}DA + r_{2b}MB - r_{3f}MA + r_{3b}GB, \\ R^{(1-\phi)\ CF}D_t^{\phi}D(t) = r_{1f}TA - r_{1b}DB - r_{2f}DA + r_{2b}MB, \\ R^{(1-\phi)\ CF}D_t^{\phi}M(t) = r_{2f}DA - r_{2b}MB - r_{3f}MA + r_{3b}GB, \\ R^{(1-\phi)\ CF}D_t^{\phi}B(t) = r_{1f}TA - r_{1b}DB + r_{2f}DA - r_{2b}MB + r_{3f}MA \\ \qquad\qquad - r_{3b}GB + \dfrac{B}{M_r}\left(1 - \dfrac{B}{B_{\max}}\right), \\ R^{(1-\phi)\ CF}D_t^{\phi}G(t) = r_{3f}MA - r_{3b}GB \end{cases} \tag{3.5}$$

with the same initial condition as above and $\phi \in (0,1]$ is the order of the CF fractional system.

3.3 ABC fractional model

For the ABC fractional operator, considering the memory rate parameter R (previously defined), the governing equations are

$$\begin{cases} R^{(1-\theta)\ ABC}D_t^{\theta}T(t) = -r_{1f}TA + r_{1b}DB, \\ R^{(1-\theta)\ ABC}D_t^{\theta}A(t) = -r_{1f}TA + r_{1b}DB - r_{2f}DA + r_{2b}MB - r_{3f}MA + r_{3b}GB, \\ R^{(1-\theta)\ ABC}D_t^{\theta}D(t) = r_{1f}TA - r_{1b}DB - r_{2f}DA + r_{2b}MB, \\ R^{(1-\theta)\ ABC}D_t^{\theta}M(t) = r_{2f}DA - r_{2b}MB - r_{3f}MA + r_{3b}GB, \\ R^{(1-\theta)\ ABC}D_t^{\theta}B(t) = r_{1f}TA - r_{1b}DB + r_{2f}DA - r_{2b}MB + r_{3f}MA \\ \qquad\qquad - r_{3b}GB + \dfrac{B}{M_r}\left(1 - \dfrac{B}{B_{\max}}\right), \\ R^{(1-\theta)\ ABC}D_t^{\theta}G(t) = r_{3f}MA - r_{3b}GB \end{cases} \tag{3.6}$$

with the same initial condition as above, i.e. $T(0) = T_0, A(0) = A_0, D(0) = 0, M(0) = 0$, $B(0) = 0$, and $G(0) = 0$ and here $\theta \in (0,1]$ represents the order of the ABC fractional derivative.

4 Existence and uniqueness of the transesterification reaction system

In this section, we establish the existence and uniqueness of solutions for the fractional model (3.6) based on the ABC derivative. The existence of solutions ensures the mathematical consistency of the ABC fractional model, confirming that solutions can be obtained under well-defined conditions. Uniqueness guarantees deterministic and unambiguous outcomes, which are essential for reliable real-world predictions. These properties validate the robustness of the model, ensuring its reliable application in biodiesel production, where precision and reproducibility are essential for optimizing reaction efficiency, improving yield, and enhancing process sustainability in industrial and environmental settings. To illustrate the existence and uniqueness of our proposed model, we employ the well-known Banach fixed-point theorem and the Arzelà-Ascoli theorem.

4.1 Existence of system

Applying the ABC integral operator to both sides of the system (3.6), we obtain

$$\begin{cases} T(t)-T(0)=R^{(\theta-1)\ ABC}I^{\theta}_{0,t}(-r_{1f}TA+r_{1b}DB), \\ A(t)-A(0)=R^{(\theta-1)\ ABC}I^{\theta}_{0,t}(-r_{1f}TA+r_{1b}DB-r_{2f}DA+r_{2b}MB-r_{3f}MA+r_{3b}GB), \\ D(t)-D(0)=R^{(\theta-1)\ ABC}I^{\theta}_{0,t}(r_{1f}TA-r_{1b}DB-r_{2f}DA+r_{2b}MB), \\ M(t)-M(0)=R^{(\theta-1)\ ABC}I^{\theta}_{0,t}(r_{2f}DA-r_{2b}MB-r_{3f}MA+r_{3b}GB), \\ B(t)-B(0)=R^{(\theta-1)\ ABC}I^{\theta}_{0,t}\Bigg(r_{1f}TA-r_{1b}DB+r_{2f}DA-r_{2b}MB+r_{3f}MA \\ \qquad\qquad -r_{3b}GB+\dfrac{B}{M_r}\left(1-\dfrac{B}{B_{\max}}\right)\Bigg), \\ G(t)-G(0)=R^{(\theta-1)\ ABC}I^{\theta}_{0,t}(r_{3f}MA-r_{3b}GB). \end{cases} \tag{4.1}$$

This implies that

$$\begin{cases} T(t)-T(0)=\dfrac{R^{(\theta-1)}(1-\theta)}{\vartheta(\theta)}\mathcal{G}_1\big(T(t),t\big)+\dfrac{R^{(\theta-1)}\theta}{\vartheta(\theta)\Gamma(\theta)}\displaystyle\int_0^t(t-s)^{\theta-1}\mathcal{G}_1\big(T(s),s\big)ds, \\ A(t)-A(0)=\dfrac{R^{(\theta-1)}(1-\theta)}{\vartheta(\theta)}\mathcal{G}_2\big(A(t),t\big)+\dfrac{R^{(\theta-1)}\theta}{\vartheta(\theta)\Gamma(\theta)}\displaystyle\int_0^t(t-s)^{\theta-1}\mathcal{G}_2\big(A(s),s\big)ds, \\ D(t)-D(0)=\dfrac{R^{(\theta-1)}(1-\theta)}{\vartheta(\theta)}\mathcal{G}_3\big(D(t),t\big)+\dfrac{R^{(\theta-1)}\theta}{\vartheta(\theta)\Gamma(\theta)}\displaystyle\int_0^t(t-s)^{\theta-1}\mathcal{G}_3\big(D(s),s\big)ds, \\ M(t)-M(0)=\dfrac{R^{(\theta-1)}(1-\theta)}{\vartheta(\theta)}\mathcal{G}_4\big(M(t),t\big)+\dfrac{R^{(\theta-1)}\theta}{\vartheta(\theta)\Gamma(\theta)}\displaystyle\int_0^t(t-s)^{\theta-1}\mathcal{G}_4\big(M(s),s\big)ds, \\ B(t)-B(0)=\dfrac{R^{(\theta-1)}(1-\theta)}{\vartheta(\theta)}\mathcal{G}_5\big(B(t),t\big)+\dfrac{R^{(\theta-1)}\theta}{\vartheta(\theta)\Gamma(\theta)}\displaystyle\int_0^t(t-s)^{\theta-1}\mathcal{G}_5\big(B(s),s\big)ds, \\ G(t)-G(0)=\dfrac{R^{(\theta-1)}(1-\theta)}{\vartheta(\theta)}\mathcal{G}_6\big(G(t),t\big)+\dfrac{R^{(\theta-1)}\theta}{\vartheta(\theta)\Gamma(\theta)}\displaystyle\int_0^t(t-s)^{\theta-1}\mathcal{G}_6\big(G(s),s\big)ds, \end{cases} \tag{4.2}$$

where the kernels $\mathcal{G}_i, i=1,2,\ldots,6$ are defined as

$$\begin{cases} \mathcal{G}_1(T(t),t) = -r_{1f}TA + r_{1b}DB, \\ \mathcal{G}_1(T(t),t) = -r_{1f}TA + r_{1b}DB - r_{2f}DA + r_{2b}MB - r_{3f}MA + r_{3b}GB, \\ \mathcal{G}_1(T(t),t) = r_{1f}TA - r_{1b}DB - r_{2f}DA + r_{2b}MB, \\ \mathcal{G}_1(T(t),t) = r_{2f}DA - r_{2b}MB - r_{3f}MA + r_{3b}GB, \\ \mathcal{G}_1(T(t),t) = r_{1f}TA - r_{1b}DB + r_{2f}DA - r_{2b}MB + r_{3f}MA - r_{3b}GB + \dfrac{B}{M_r}\left(1 - \dfrac{B}{B_{\max}}\right), \\ \mathcal{G}_1(T(t),t) = r_{3f}MA - r_{3b}GB. \end{cases}$$

Let $\mathcal{L}$ be the linear operator acting on the entire system (4.2), defined as

$$\begin{cases} \mathcal{L}\big(T(t)\big) = \dfrac{R^{(\theta-1)}(1-\theta)}{\vartheta(\theta)}\mathcal{G}_1\big(T(t),t\big) + \dfrac{R^{(\theta-1)}\theta}{\vartheta(\theta)\Gamma(\theta)}\displaystyle\int_0^t (t-s)^{\theta-1}\mathcal{G}_1\big(T(s),s\big)ds, \\ \mathcal{L}\big(A(t)\big) = \dfrac{R^{(\theta-1)}(1-\theta)}{\vartheta(\theta)}\mathcal{G}_2\big(A(t),t\big) + \dfrac{R^{(\theta-1)}\theta}{\vartheta(\theta)\Gamma(\theta)}\displaystyle\int_0^t (t-s)^{\theta-1}\mathcal{G}_2\big(A(s),s\big)ds, \\ \mathcal{L}\big(D(t)\big) = \dfrac{R^{(\theta-1)}(1-\theta)}{\vartheta(\theta)}\mathcal{G}_3\big(D(t),t\big) + \dfrac{R^{(\theta-1)}\theta}{\vartheta(\theta)\Gamma(\theta)}\displaystyle\int_0^t (t-s)^{\theta-1}\mathcal{G}_3\big(D(s),s\big)ds, \\ \mathcal{L}\big(M(t)\big) = \dfrac{R^{(\theta-1)}(1-\theta)}{\vartheta(\theta)}\mathcal{G}_4\big(M(t),t\big) + \dfrac{R^{(\theta-1)}\theta}{\vartheta(\theta)\Gamma(\theta)}\displaystyle\int_0^t (t-s)^{\theta-1}\mathcal{G}_4\big(M(s),s\big)ds, \\ \mathcal{L}\big(B(t)\big) = \dfrac{R^{(\theta-1)}(1-\theta)}{\vartheta(\theta)}\mathcal{G}_5\big(B(t),t\big) + \dfrac{R^{(\theta-1)}\theta}{\vartheta(\theta)\Gamma(\theta)}\displaystyle\int_0^t (t-s)^{\theta-1}\mathcal{G}_5\big(B(s),s\big)ds, \\ \mathcal{L}\big(G(t)\big) = \dfrac{R^{(\theta-1)}(1-\theta)}{\vartheta(\theta)}\mathcal{G}_6\big(G(t),t\big) + \dfrac{R^{(\theta-1)}\theta}{\vartheta(\theta)\Gamma(\theta)}\displaystyle\int_0^t (t-s)^{\theta-1}\mathcal{G}_6\big(G(s),s\big)ds. \end{cases} \tag{4.3}$$

Now we have to prove that $\mathcal{L}(H)$, where $H=[T(t),A(t),D(t),M(t),B(t),G(t)]^\top$ is compact to ensure the existence and boundedness of the solutions of the system (3.6). Consider the first equation of the system (4.3), we can write,

$$\begin{aligned} \big\|\mathcal{L}\big(T(t)\big)\big\| &= \left\| \frac{R^{(\theta-1)}(1-\theta)}{\vartheta(\theta)}\mathcal{G}_1\big(T(t),t\big) + \frac{R^{(\theta-1)}\theta}{\vartheta(\theta)\Gamma(\theta)}\int_0^t (t-s)^{\theta-1}\mathcal{G}_1\big(T(s),s\big)ds \right\|, \\ &\le \frac{R^{(\theta-1)}(1-\theta)}{\vartheta(\theta)}\big\|\mathcal{G}_1\big(T(t),t\big)\big\| + \frac{R^{(\theta-1)}\theta}{\vartheta(\theta)\Gamma(\theta)}\left\| \int_0^t (t-s)^{\theta-1}\mathcal{G}_1\big(T(s),s\big)ds \right\|, \\ &= \frac{R^{(\theta-1)}(1-\theta)}{\vartheta(\theta)}\big\|\mathcal{G}_1\big(T(t),t\big)\big\| + \frac{R^{(\theta-1)}T^\theta}{\vartheta(\theta)\Gamma(\theta)}\left\| \int_0^t \mathcal{G}_1\big(T(s),s\big)ds \right\|, \\ &\le \left[\frac{R^{(\theta-1)}(1-\theta)}{\vartheta(\theta)} + K_1\frac{R^{(\theta-1)}T^\theta}{\vartheta(\theta)\Gamma(\theta)}\right]\big\|\mathcal{G}_1\big(T(t),t\big)\big\|. \end{aligned} \tag{4.4}$$

We can assume that there exist positive real numbers $\nu_1,\nu_2,\nu_3,\nu_4,\nu_4$, and ν_6 such that

$$\|T(t)\| \le \nu_1, \quad \|A(t)\| \le \nu_2, \quad \|D(t)\| \le \nu_3, \quad \|M(t)\| \le \nu_4, \quad \|B(t)\| \le \nu_5, \quad \|G(t)\| \le \nu_6.$$

Let

$$\mathcal{B}_1 = \max_{\substack{t\in[0,T]\\ T\in[0,\nu_1]}} \mathcal{G}_1\big(T(t),t\big),$$

and utilizing this in the Eq. 4.4, we get

$$\big\|\mathcal{L}\big(T(t)\big)\big\| \le \mathcal{B}_1\left[\frac{R^{(\theta-1)}(1-\theta)}{\vartheta(\theta)} + K_1\frac{R^{(\theta-1)}T^{\theta}}{\vartheta(\theta)\Gamma(\theta)}\right]. \tag{4.5}$$

Proceeding similarly, we can obtain that

$$\begin{aligned}
\big\|\mathcal{L}\big(A(t)\big)\big\| &\le \mathcal{B}_2\left[\frac{R^{(\theta-1)}(1-\theta)}{\vartheta(\theta)} + K_2\frac{R^{(\theta-1)}T^{\theta}}{\vartheta(\theta)\Gamma(\theta)}\right],\\
\big\|\mathcal{L}\big(D(t)\big)\big\| &\le \mathcal{B}_3\left[\frac{R^{(\theta-1)}(1-\theta)}{\vartheta(\theta)} + K_3\frac{R^{(\theta-1)}T^{\theta}}{\vartheta(\theta)\Gamma(\theta)}\right],\\
\big\|\mathcal{L}\big(M(t)\big)\big\| &\le \mathcal{B}_4\left[\frac{R^{(\theta-1)}(1-\theta)}{\vartheta(\theta)} + K_4\frac{R^{(\theta-1)}T^{\theta}}{\vartheta(\theta)\Gamma(\theta)}\right],\\
\big\|\mathcal{L}\big(B(t)\big)\big\| &\le \mathcal{B}_5\left[\frac{R^{(\theta-1)}(1-\theta)}{\vartheta(\theta)} + K_5\frac{R^{(\theta-1)}T^{\theta}}{\vartheta(\theta)\Gamma(\theta)}\right],\\
\big\|\mathcal{L}\big(G(t)\big)\big\| &\le \mathcal{B}_6\left[\frac{R^{(\theta-1)}(1-\theta)}{\vartheta(\theta)} + K_6\frac{R^{(\theta-1)}T^{\theta}}{\vartheta(\theta)\Gamma(\theta)}\right],
\end{aligned}$$

where

$$\begin{aligned}
\mathcal{B}_2 &= \max_{\substack{t\in[0,T]\\ A\in[0,\nu_2]}} \mathcal{G}_2\big(A(t),t\big), \quad \mathcal{B}_3 = \max_{\substack{t\in[0,T]\\ D\in[0,\nu_3]}} \mathcal{G}_3\big(D(t),t\big),\\
\mathcal{B}_4 &= \max_{\substack{t\in[0,T]\\ M\in[0,\nu_4]}} \mathcal{G}_4\big(M(t),t\big), \quad \mathcal{B}_5 = \max_{\substack{t\in[0,T]\\ B\in[0,\nu_5]}} \mathcal{G}_5\big(B(t),t\big),\\
\mathcal{B}_6 &= \max_{\substack{t\in[0,T]\\ G\in[0,\nu_6]}} \mathcal{G}_6\big(G(t),t\big).
\end{aligned}$$

Therefore, $\mathcal{L}(H)$ is bounded. Let us consider $t_2 > t_1$ and for a given $\epsilon > 0$, there exist a $\delta > 0$ such that $\|t_2 - t_2\| < \delta$. Now we can write for that first equation as

$$\begin{aligned}
&\big\|\mathcal{G}_1\big(T(t_2),t_2\big) - \mathcal{G}_1\big(T(t_1),t_1\big)\big\|\\
&= \big\|\big(-r_{1f}T(t_2)A(t) + r_{1b}D(t)B(t)\big) - \big(-r_{1f}T(t_1)A(t) + r_{1b}D(t)B(t)\big)\big\|\\
&\le r_{1f}\nu_2\|T(t_2) - T(t_1)\|.
\end{aligned} \tag{4.6}$$

Assuming that if the function $T(t)$ is Lipschitz continuous, i.e. there exists for some real number $\chi_1 > 0$ and for all t_2, t_1, the inequality

$$\|T(t_2) - T(t_1)\| \le \chi_1\|t_2 - t_1\|$$

holds. We rewrite the Eq. (4.6) as,

$$\left\|\mathcal{G}_1\left(T(t_2),t_2\right)-\mathcal{G}_1\left(T(t_1),t_1\right)\right\|\leq\mathcal{R}_1\|t_2-t_1\|, \tag{4.7}$$

where $\mathcal{R}_1=r_{1f}\nu_2\chi_1$. Similarly, if the other population of the system $A(t),D(t),G(t),B(t)$, and $G(t)$ are Lipschitz continuous, then there exist some positive real numbers $\mathcal{R}_i$, $i=2,3,\ldots,6$, for which we can write as following:

$$\begin{aligned}
&\left\|\mathcal{G}_2\left(A(t_2),t_2\right)-\mathcal{G}_2\left(A(t_1),t_1\right)\right\|\leq\mathcal{R}_2\|t_2-t_1\|,\\
&\left\|\mathcal{G}_3\left(D(t_2),t_2\right)-\mathcal{G}_3\left(D(t_1),t_1\right)\right\|\leq\mathcal{R}_3\|t_2-t_1\|,\\
&\left\|\mathcal{G}_4\left(M(t_2),t_2\right)-\mathcal{G}_4\left(M(t_1),t_1\right)\right\|\leq\mathcal{R}_4\|t_2-t_1\|,\\
&\left\|\mathcal{G}_5\left(B(t_2),t_2\right)-\mathcal{G}_5\left(B(t_1),t_1\right)\right\|\leq\mathcal{R}_5\|t_2-t_1\|,\\
&\left\|\mathcal{G}_6\left(G(t_2),t_2\right)-\mathcal{G}_6\left(G(t_1),t_1\right)\right\|\leq\mathcal{R}_6\|t_2-t_1\|.
\end{aligned} \tag{4.8}$$

Furthermore, using the Eq. (4.4) with the inequality (4.7), we have

$$\begin{aligned}
&\left\|\mathcal{L}\left(T(t_2)\right)-\mathcal{L}\left(T(t_1)\right)\right\|\\
&\leq\left\|\left[\frac{R^{(\theta-1)}(1-\theta)}{\vartheta(\theta)}+K_1\frac{R^{(\theta-1)}T^{\theta}}{\vartheta(\theta)\Gamma(\theta)}\right]\left(\mathcal{G}_1\left(T(t_2),t_2\right)-\mathcal{G}_1\left(T(t_1),t_1\right)\right)\right\|,\\
&\leq\left[\frac{R^{(\theta-1)}(1-\theta)}{\vartheta(\theta)}+K_1\frac{R^{(\theta-1)}T^{\theta}}{\vartheta(\theta)\Gamma(\theta)}\right]\mathcal{R}_1\|t_2-t_1\|.
\end{aligned} \tag{4.9}$$

Choosing

$$\delta=\frac{\epsilon}{\left[R^{(\theta-1)}(1-\theta)/\vartheta(\theta)+K_1R^{(\theta-1)}T^{\theta}/\left(\vartheta(\theta)\Gamma(\theta)\right)\right]\mathcal{R}_1},$$

and we can see that $\|\mathcal{L}(T(t_2))-\mathcal{L}(T(t_1))\|<\epsilon$ whenever $\|t_2-t_1\|<\delta$. Proceeding similarly, we can show that $\|\mathcal{L}(H(t_2))-\mathcal{L}(H(t_1))\|<\epsilon$ where $H=[A(t),D(t),M(t),B(t),G(t)]^{\top}$. Hence, according to the Arzela-Ascoli theorem [15], we can say that the operator $\mathcal{L}(H)$ is compact. Therefore, the solutions of the fractional system (3.6), corresponding to the method exist. Now we prove the uniqueness of this solution in the subsequent section.

4.2 Uniqueness of system

Let $T(t)$ and $T'(t)$ be the two solutions of the fractional system (3.6). Then for the first population, we can write as

$$\left\|\mathcal{G}_1\left(T(t),t\right)-\mathcal{G}_1\left(T'(t),t\right)\right\|=\left\|-r_{1f}A(t)\left(T(t)-T'(t)\right)\right\|\leq\Delta_1\|T(t)-T'(t)\|, \tag{4.10}$$

where $\Delta_1 = r_{1f}v_1$. Similarly, we obtain for the other population as follows:

$$\begin{cases} \|\mathcal{G}_2(A(t),t) - \mathcal{G}_2(A'(t),t)\| \leq \Delta_2 \|A(t) - A'(t)\|, \\ \|\mathcal{G}_3(D(t),t) - \mathcal{G}_3(D'(t),t)\| \leq \Delta_3 \|D(t) - D'(t)\|, \\ \|\mathcal{G}_4(M(t),t) - \mathcal{G}_4(M'(t),t)\| \leq \Delta_4 \|M(t) - M'(t)\|, \\ \|\mathcal{G}_5(B(t),t) - \mathcal{G}_5(B'(t),t)\| \leq \Delta_5 \|B(t) - B'(t)\|, \\ \|\mathcal{G}_6(G(t),t) - \mathcal{G}_6(G'(t),t)\| \leq \Delta_6 \|G(t) - G'(t)\|. \end{cases}$$

Now we prove the uniqueness of the solution of the system (3.6). For this, let us consider the linear operator $\mathcal{L}$ again, which is defined in the previous section and using the relation in Eq. (4.10). We obtain

$$\begin{aligned} &\|\mathcal{L}(T(t)) - \mathcal{L}(T'(t))\| \\ &= \left\| \frac{R^{(\theta-1)}(1-\theta)}{\vartheta(\theta)} (\mathcal{G}_1(T(t),t) - \mathcal{G}_1(T'(t),t)) \right. \\ &\quad \left. + \frac{R^{(\theta-1)}\theta}{\vartheta(\theta)\Gamma(\theta)} \int_0^t (t-s)^{\theta-1} (\mathcal{G}_1(T(s),s) - \mathcal{G}_1(T'(s),s)) ds \right\| \\ &\leq \frac{R^{(\theta-1)}(1-\theta)}{\vartheta(\theta)} \|\mathcal{G}_1(T(t),t) - \mathcal{G}_1(T'(t),t)\| \\ &\quad + \frac{R^{(\theta-1)}T^{\theta}}{\vartheta(\theta)\Gamma(\theta)} \left\| \int_0^t \mathcal{G}_1(T(s),s) - \mathcal{G}_1(T'(s),s) ds \right\| \\ &\leq \left[\frac{R^{(\theta-1)}(1-\theta)}{\vartheta(\theta)} \Delta_1 + K_1 \frac{R^{(\theta-1)}T^{\theta}}{\vartheta(\theta)\Gamma(\theta)} \Delta_1 \right] \|T(t) - T'(t)\|. \end{aligned}$$

Proceeding similarly for other equations, we can obtain

$$\begin{cases} \|\mathcal{L}(A(t)) - \mathcal{L}(A'(t))\| \leq \left[\frac{R^{(\theta-1)}(1-\theta)}{\vartheta(\theta)} \Delta_2 + K_2 \frac{R^{(\theta-1)}T^{\theta}}{\vartheta(\theta)\Gamma(\theta)} \Delta_2 \right] \|A(t) - A'(t)\|, \\ \|\mathcal{L}(D(t)) - \mathcal{L}(D'(t))\| \leq \left[\frac{R^{(\theta-1)}(1-\theta)}{\vartheta(\theta)} \Delta_3 + K_3 \frac{R^{(\theta-1)}T^{\theta}}{\vartheta(\theta)\Gamma(\theta)} \Delta_3 \right] \|D(t) - D'(t)\|, \\ \|\mathcal{L}(M(t)) - \mathcal{L}(M'(t))\| \leq \left[\frac{R^{(\theta-1)}(1-\theta)}{\vartheta(\theta)} \Delta_4 + K_4 \frac{R^{(\theta-1)}T^{\theta}}{\vartheta(\theta)\Gamma(\theta)} \Delta_4 \right] \|M(t) - M'(t)\|, \\ \|\mathcal{L}(B(t)) - \mathcal{L}(B'(t))\| \leq \left[\frac{R^{(\theta-1)}(1-\theta)}{\vartheta(\theta)} \Delta_5 + K_5 \frac{R^{(\theta-1)}T^{\theta}}{\vartheta(\theta)\Gamma(\theta)} \Delta_5 \right] \|B(t) - B'(t)\|, \\ \|\mathcal{L}(G(t)) - \mathcal{L}(G'(t))\| \leq \left[\frac{R^{(\theta-1)}(1-\theta)}{\vartheta(\theta)} \Delta_6 + K_6 \frac{R^{(\theta-1)}T^{\theta}}{\vartheta(\theta)\Gamma(\theta)} \Delta_6 \right] \|G(t) - G'(t)\|. \end{cases}$$

The linear operator $\mathcal{L}$ will be a contraction mapping if the following conditions are hold:

$$\begin{cases} \dfrac{R^{(\theta-1)}(1-\theta)}{\vartheta(\theta)}\Delta_1+K_1\dfrac{R^{(\theta-1)}T^{\theta}}{\vartheta(\theta)\Gamma(\theta)}\Delta_1<1, \\ \dfrac{R^{(\theta-1)}(1-\theta)}{\vartheta(\theta)}\Delta_2+K_2\dfrac{R^{(\theta-1)}T^{\theta}}{\vartheta(\theta)\Gamma(\theta)}\Delta_2<1, \\ \dfrac{R^{(\theta-1)}(1-\theta)}{\vartheta(\theta)}\Delta_3+K_3\dfrac{R^{(\theta-1)}T^{\theta}}{\vartheta(\theta)\Gamma(\theta)}\Delta_3<1, \\ \dfrac{R^{(\theta-1)}(1-\theta)}{\vartheta(\theta)}\Delta_4+K_4\dfrac{R^{(\theta-1)}T^{\theta}}{\vartheta(\theta)\Gamma(\theta)}\Delta_4<1, \\ \dfrac{R^{(\theta-1)}(1-\theta)}{\vartheta(\theta)}\Delta_5+K_5\dfrac{R^{(\theta-1)}T^{\theta}}{\vartheta(\theta)\Gamma(\theta)}\Delta_5<1, \\ \dfrac{R^{(\theta-1)}(1-\theta)}{\vartheta(\theta)}\Delta_6+K_6\dfrac{R^{(\theta-1)}T^{\theta}}{\vartheta(\theta)\Gamma(\theta)}\Delta_6<1. \end{cases} \tag{4.11}$$

Therefore, the fixed point theory [25] ensures the uniqueness of the solution of system (3.6) if all the condition in Eq. (4.11) are satisfied.

5 Fractional optimal-control problem

In this section, we examine the formulation and solution of an optimal control problem by using ABC operator for the model (3.6). Developing optimal control problems (OCP) for various real-world phenomena is a growing and dynamic research field. Generally, the formulation of a fractional optimal control problem (see Fig. 2) involves first determining the optimal control $z(t)$, that minimizes the cost function

$$J(z)=\int_{t_0}^{t_f} G(t,y,z)dt$$

subject to the constraint

$$R^{(1-\theta)\,ABC}D_t^{\theta}y=F(t,y,z)$$

with initial condition $y(0)=y_0$, where $0<\theta\leq 1$, the state and control variables y and z respectively, $G(t,y,z)$ and $F(t,y,z)$ are differentiable functions.

In this model, we considered the state variable as $y=(T,A,D,M,B,G)\in R^6$, and we aim to find the optimal control $z^*(t)\in R$ to minimize the mass-transfer resistance between methanol and WCO. Let us consider the following cost functional:

$$J[z]=\int_{t_0}^{t_f}\left[W_1z^2-W_2B^2\right]dt,$$

where W_1 represents the weight constant with $W_1>0$, while W_2 stands for the penalty multiplier. Let the control input variable $z(t)$ represent the ultrasonic frequency applied

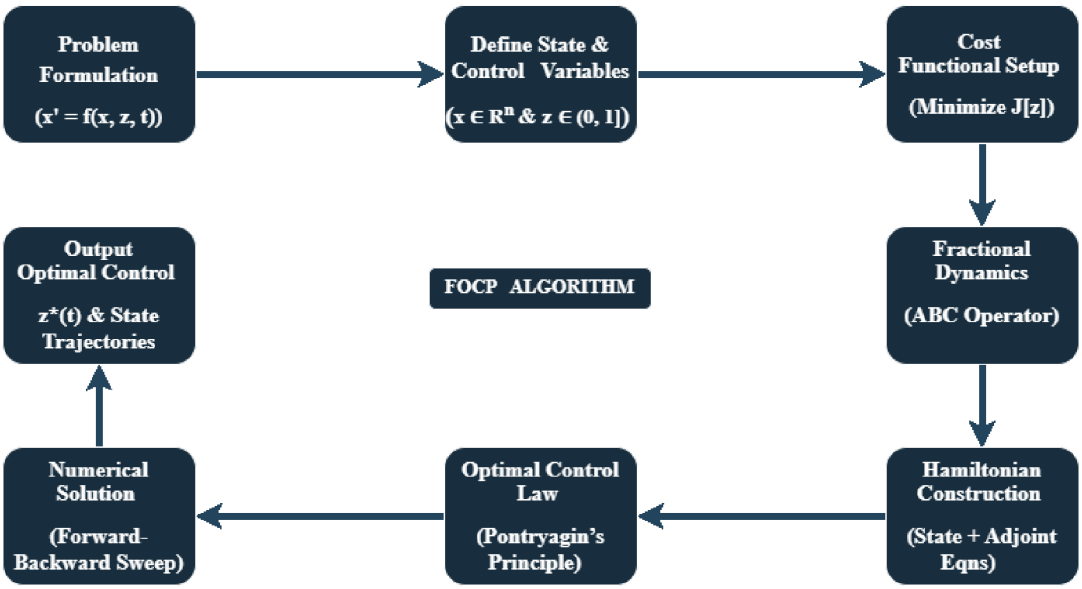

Figure 2: Flowchart of the fractional optimal control problem algorithm, illustrating the sequential steps from problem formulation to the derivation of optimal control and state trajectories using the Atangana-Baleanu (ABC) fractional operator and Pontryagin's principle.

at time t, where $0\leq z(t)\leq 1$. A value of $z(t)=1$ corresponds to the maximum utilization of ultrasound frequency, while $z(t)=0$ signifies no ultrasound application. Hence, the model system of equations (3.6) becomes

$$\begin{cases} F_1 = R^{(1-\theta)^{ABC}}D_t^\theta T(t) = -r_{1f}TA + r_{1b}DB, \\ F_2 = R^{(1-\theta)^{ABC}}D_t^\theta A(t) = -r_{1f}TA + r_{1b}DB - r_{2f}DA + r_{2b}MB - r_{3f}MA + r_{3b}GB, \\ F_3 = R^{(1-\theta)^{ABC}}D_t^\theta D(t) = r_{1f}TA - r_{1b}DB - r_{2f}DA + r_{2b}MB, \\ F_4 = R^{(1-\theta)^{ABC}}D_t^\theta M(t) = r_{2f}DA - r_{2b}MB - r_{3f}MA + r_{3b}GB, \\ F_5 = R^{(1-\theta)^{ABC}}D_t^\theta B(t) = r_{1f}TA - r_{1b}DB + r_{2f}DA - r_{2b}MB + r_{3f}MA \\ \qquad\qquad - r_{3b}GB + \dfrac{B}{zM_r}\left(1 - \dfrac{B}{B_{\max}}\right), \\ F_6 = R^{(1-\theta)^{ABC}}D_t^\theta G(t) = r_{3f}MA - r_{3b}GB \end{cases} \tag{5.1}$$

with initial conditions $T(0)=T_0, A(0)=A_0, D(0)=0, M(0)=0, B(0)=0$, and $G(0)=0$. Our objective is to find the optimal control $z^*(t)$ that minimizes the functional $J(z)$, i.e.

$$J(z^*) = \min\{J(z) : z \in Z\}.$$

The set Z of feasible controls, consists of all measurable functions satisfying

$$Z = \{z \mid z \text{ is measurable and satisfies } 0\leq z\leq 1, \forall t \in [t_0, t_f]\}.$$

To determine $z^*(t)$, we utilize Pontryagin's minimum principle [18]. The Hamiltonian is expressed as

$$\begin{aligned}\mathcal{H} &= W_1 z^2 - W_2 B^2 + \sum_{n=1}^{6} \Phi_i F_i, \\ &= W_1 z^2 - W_2 B^2 + \Phi_T(-r_{1f}TA + r_{1b}DB) \\ &\quad + \Phi_A(-r_{1f}TA + r_{1b}DB - r_{2f}DA + r_{2b}MB - r_{3f}MA + r_{3b}GB) \\ &\quad + \Phi_D(r_{1f}TA - r_{1b}DB - r_{2f}DA + r_{2b}MB) \\ &\quad + \Phi_M(r_{2f}DA - r_{2b}MB - r_{3f}MA + r_{3b}GB) \\ &\quad + \Phi_B\left(r_{1f}TA - r_{1b}DB + r_{2f}DA - r_{2b}MB + r_{3f}MA - r_{3b}GB + \frac{B}{zM_r}\left(1 - \frac{B}{B_{\max}}\right)\right) \\ &\quad + \Phi_G(r_{3f}MA - r_{3b}GB), \end{aligned} \tag{5.2}$$

where $\Phi_T, \Phi_A, \cdots, \Phi_G$ are adjoint variables and $F_1, F_2, \cdots, F_6$ are functions defined in Eq. (5.1) with the properties

$$\begin{cases} R^{(1-\theta)}D_t^\theta \Phi_T = -\dfrac{\partial \mathcal{H}}{\partial T} = r_{1f}A(\Phi_A + \Phi_T - \Phi_D - \Phi_B), \\ R^{(1-\theta)ABC}D_t^\theta \Phi_A = -\dfrac{\partial \mathcal{H}}{\partial A} = r_{1f}T(\Phi_A + \Phi_T - \Phi_D - \Phi_B) + r_{2f}D(\Phi_A + \Phi_D - \Phi_M - \Phi_B) \\ \qquad\qquad + r_{3f}M(\Phi_A + \Phi_M - \Phi_B - \Phi_G), \\ R^{(1-\theta)ABC}D_t^\theta \Phi_D = -\dfrac{\partial \mathcal{H}}{\partial D} = r_{1b}B(-\Phi_A - \Phi_T + \Phi_D + \Phi_B) \\ \qquad\qquad + r_{2f}A(\Phi_A + \Phi_D - \Phi_M - \Phi_B), \\ R^{(1-\theta)ABC}D_t^\theta \Phi_M = -\dfrac{\partial \mathcal{H}}{\partial M} = r_{2b}B(-\Phi_A - \Phi_D + \Phi_M + \Phi_B) \\ \qquad\qquad + r_{3f}A(\Phi_A + \Phi_M - \Phi_B - \Phi_G), \\ R^{(1-\theta)ABC}D_t^\theta \Phi_B = -\dfrac{\partial \mathcal{H}}{\partial B} = 2W_2 B + r_{1b}D(-\Phi_A - \Phi_T + \Phi_D + \Phi_B) \\ \qquad\qquad + r_{2b}M(-\Phi_A - \Phi_D + \Phi_M + \Phi_B) \\ \qquad\qquad + r_{3b}G(-\Phi_A - \Phi_M + \Phi_B + \Phi_G) - \dfrac{1}{zM_r}\left(1 - \dfrac{2B}{B_{\max}}\right), \\ R^{(1-\theta)ABC}D_t^\theta \Phi_G = -\dfrac{\partial \mathcal{H}}{\partial G} = r_{3b}B(-\Phi_A - \Phi_M + \Phi_B + \Phi_G). \end{cases} \tag{5.3}$$

The transversality conditions are

$$\Phi_T(t_f) = \Phi_A(t_f) = \Phi_D(t_f) = \Phi_M(t_f) = \Phi_B(t_f) = \Phi_G(t_f) = 0.$$

Theorem 5.1. *The control parameter z^* that minimizes $J(z)$ over Z are given by*

$$z^*(t) = \max\left(0, \min\left(1, \left\{\frac{\Phi_B B(B_{\max} - B)}{2W_1 M_r B_{\max}}\right\}^{\frac{1}{3}}\right)\right),$$

where $\Phi_T, \Phi_A, \Phi_D, \Phi_M, \Phi_B, \Phi_G$ *are the adjoint variables satisfying Eqs.* (5.3) *and the following transversality conditions:*

$$\Phi_T(0)=\Phi_A(0)=\Phi_D(0)=\Phi_M(0)=\Phi_B(0)=\Phi_G(0)=0,$$

and

$$z^*(t)=\begin{cases}0, & \left\{\frac{\Phi_B B(B_{max}-B)}{2W_1 M_r B_{max}}\right\}^{\frac{1}{3}}\leq 0,\\ \left\{\frac{\Phi_B B(B_{max}-B)}{2W_1 M_r B_{max}}\right\}^{\frac{1}{3}}, & 0<\left\{\frac{\Phi_B B(B_{max}-B)}{2W_1 M_r B_{max}}\right\}^{\frac{1}{3}}<1,\\ 1, & \left\{\frac{\Phi_B B(B_{max}-B)}{2W_1 M_r B_{max}}\right\}^{\frac{1}{3}}\geq 1.\end{cases}$$

Proof. Differentiating the Hamiltonian (5.2) with respect to z, we get

$$\frac{\partial H}{\partial z^*}=0=2W_1 z^*-\frac{\Phi_B B(B_{\max}-B)}{2W_1 M_r^\theta B_{\max} z^{*2}} \implies z^*=\left\{\frac{\Phi_B B(B_{\max}-B)}{2W_1 M_r^\theta B_{\max}}\right\}^{\frac{1}{3}}.$$

Applying the Pontryagin minimum principle, we get

$$R^{(1-\theta)ABC}D_t^\theta\Phi_T=-\frac{\partial\mathcal{H}}{\partial T},\quad R^{(1-\theta)ABC}D_t^\theta\Phi_A=-\frac{\partial\mathcal{H}}{\partial A},\quad R^{(1-\theta)ABC}D_t^\theta\Phi_D=-\frac{\partial\mathcal{H}}{\partial D},$$
$$R^{(1-\theta)ABC}D_t^\theta\Phi_M=-\frac{\partial\mathcal{H}}{\partial M},\quad R^{(1-\theta)ABC}D_t^\theta\Phi_A=-\frac{\partial\mathcal{H}}{\partial B},\quad R^{(1-\theta)ABC}D_t^\theta\Phi_G=-\frac{\partial\mathcal{H}}{\partial G}$$

with transversality condition

$$\Phi_T(t_f)=\Phi_A(t_f)=\Phi_D(t_f)=\Phi_M(t_f)=\Phi_B(t_f)=\Phi_G(t_f)=0.$$

The proof is complete. □

6 Numerical validation

This section presents the numerical illustration of our biodiesel model results. We employ MATLAB 2021a and Python for the numerical simulations. First, we outline the complete numerical scheme corresponding to different fractional derivative operators, specifically the ABC derivative and the CF derivative. The numerical solution uses these numerical schemes to analyze the model's behavior effectively.

6.1 Numerical solution scheme for reaction system

6.1.1 ABC fractional operator

The fractional system (3.6) corresponding to Atangana-Baleanu in the Caputo sense can be written as

$$R^{1-\theta\ ABC}D_t^\theta\big(f(t)\big)=\Psi\big(t,f(t)\big),\tag{6.1}$$

where $f(t)=[T(t),A(t),D(t),M(t),B(t),G(t)]^\top$ and $\Psi(t,f(t))$ denotes the right-hand side of the fractional system (3.6). Applying the Definition 2.4, in the Eq. (6.1), we get

$$f(t)-f(0)=\frac{R^{(\theta-1)}(1-\theta)}{\vartheta(\theta)}\Psi\big(f(t),t\big)+\frac{R^{(\theta-1)}\theta}{\vartheta(\theta)\Gamma(\theta)}\int_0^t(t-s)^{\theta-1}\Psi\big(f(s),s\big)ds.$$

Using iteration, the equation is reformulated as

$$\begin{aligned}f(t_{n+1})=f(0)&+\frac{R^{(\theta-1)}(1-\theta)}{\vartheta(\theta)}\Psi\big(f(t_n),t_n\big)\\&+\frac{R^{(\theta-1)}\theta}{\vartheta(\theta)\Gamma(\theta)}\sum_{k=0}^{n}\int_{t_k}^{t_{k+1}}(t_{n+1}-s)^{\theta-1}\Psi\big(f(s),s\big)ds.\end{aligned}\tag{6.2}$$

Utilizing the two-step Lagrange interpolation polynomial, the function $\Psi(f(s),s)$ approximated in the interval $[t_k,t_{k+1}]$ as follows:

$$\Psi\big(f(s),s\big)\approx\frac{\Psi\big(f(t_k),t_k\big)}{h}(s-t_{k-1})-\frac{\Psi\big(f(t_{k-1}),t_{k-1}\big)}{h}(s-t_k),\tag{6.3}$$

where h is the time step size. Now,

$$\begin{aligned}&\int_{t_k}^{t_{k+1}}(t_{n+1}-s)^{\theta-1}\Psi\big(f(s),s\big)ds,\\&=\int_{t_k}^{t_{k+1}}\left[(t_{n+1}-s)^{\theta-1}(s-t_{k-1})\frac{\Psi\big(f(t_k),t_k\big)}{h}-(t_{n+1}-s)^{\theta-1}(s-t_k)\frac{\Psi\big(f(t_{k-1}),t_{k-1}\big)}{h}\right]ds,\\&=\frac{h^\theta}{\theta(\theta+1)}\big[(n-k+1)^\theta(n-k+\theta+2)-(n-k)^\theta(n-k+2\theta+2)\big]\Psi\big(f(t_k),t_k\big)\\&\quad-\frac{h^\theta}{\theta(\theta+1)}\big[(n-k+1)^{\theta+1}-(n-k)^\theta(n-k+\theta+1)\big]\Psi\big(f(t_{k-1}),t_{k-1}\big).\end{aligned}$$

Using this result in the Eq. (6.2), we have the numerical solution of the fractional system (3.6) corresponding to Atangana-Baleanu in the Caputo sense, as follows:

$$\begin{aligned}f(t_{n+1})=f(0)&+\frac{R^{(\theta-1)}(1-\theta)}{\vartheta(\theta)}\Psi\big(f(t_n),t_n\big)+\frac{R^{(\theta-1)}h^\theta}{\vartheta(\theta)\Gamma(\theta)(\theta+1)}\\&\times\sum_{k=0}^{n}\Big[\big[(n-k+1)^\theta(n-k+\theta+2)-(n-k)^\theta(n-k+2\theta+2)\big]\Psi\big(f(t_k),t_k\big)\\&\qquad-\big[(n-k+1)^{\theta+1}-(n-k)^\theta(n-k+\theta+1)\big]\Psi\big(f(t_{k-1}),t_{k-1}\big)\Big].\end{aligned}\tag{6.4}$$

6.1.2 Caputo-Fabrizio fractional operator

The fractional system (3.5) corresponding to CF differential operator can be written as

$$R^{1-\phi\ CF}D_t^\phi\big(g(t)\big)=\Psi'\big(g(t),t\big),\tag{6.5}$$

where $g(t)=[T(t),A(t),D(t),M(t),B(t),G(t)]^\top$ and $\Psi'(t,g(t))$ denotes the right-hand side of the fractional system (3.5). Applying the fundamental theorem in the Eq. (6.5), we obtain

$$g(t)-g(0)=\frac{R^{(\phi-1)}(1-\phi)}{M(\phi)}\Psi'\big(g(t),t\big)+\frac{R^{(\phi-1)}\phi}{M(\phi)}\int_0^t\Psi'\big(g(s'),s'\big)ds'.$$

Now this equation can be written as follows:

$$\begin{cases} g(t_{n+1})-g(0)=\dfrac{R^{(\phi-1)}(1-\phi)}{M(\phi)}\Psi'\big(g(t_n),t_n\big)+\dfrac{R^{(\phi-1)}\phi}{M(\phi)}\displaystyle\int_0^{t_{n+1}}\Psi'\big(g(s'),s'\big)ds', \\ g(t_n)-g(0)=\dfrac{R^{(\phi-1)}(1-\phi)}{M(\phi)}\Psi'\big(g(t_{n-1}),t_{n-1}\big)+\dfrac{R^{(\phi-1)}\phi}{M(\phi)}\displaystyle\int_0^{t_n}\Psi'\big(g(s'),s'\big)ds'. \end{cases}$$

Replacing the second equation in the first equation, we obtain

$$\begin{aligned} g(t_{n+1})-g(t_n)=&\frac{R^{(\phi-1)}(1-\phi)}{M(\phi)}\big(\Psi'\big(g(t_n),t_n\big)-\Psi'\big(g(t_{n-1}),t_{n-1}\big)\big)\\ &+\frac{R^{(\phi-1)}\phi}{M(\phi)}\int_{t_n}^{t_{n+1}}\Psi'\big(g(s'),s'\big)ds'. \end{aligned}\tag{6.6}$$

Utilizing the result as in Eq. (6.3), we have

$$\int_{t_n}^{t_{n+1}}\Psi'\big(g(s'),s'\big)ds'=\frac{3h}{2}\Psi'\big(g(t_n),t_n\big)-\frac{h}{2}\Psi'\big(g(t_{n-1}),t_{n-1}\big),\tag{6.7}$$

where h is the time step size. Therefore, using two Eqs. (6.6) and (6.7), we get the numerical solution for the CF fractional system (6.5) as follows:

$$\begin{aligned} g(t_{n+1})=g(t_n)+\frac{R^{(\phi-1)}}{M(\phi)}\Bigg[&\left(1-\phi+\frac{3h\phi}{2}\right)\Psi'\big(g(t_n),t_n\big)\\ &-\left(1-\phi+\frac{h\phi}{2}\right)\Psi'\big(g(t_{n-1}),t_{n-1}\big)\Bigg]. \end{aligned}\tag{6.8}$$

6.2 Sensitivity analysis of reaction parameters

To assess the impact of model parameters on the biodiesel production system, we perform a sensitivity analysis using the Pearson correlation coefficient method. Sensitivity analysis plays a crucial role in determining how variations in input parameters influence the system's output, thereby identifying key parameters that significantly affect the biodiesel yield and efficiency.

Uncertainty analysis is essential for assessing the reliability and sensitivity of system parameters in biodiesel production. The Pearson correlation coefficient (PCC) is a key statistical measure that quantifies the strength and direction of the linear relationship between input parameters and model outputs. Unlike rank-based methods, PCC evaluates

direct proportionality, helping identify dominant parameters that significantly influence system behavior. By performing uncertainty analysis, we can quantify parameter sensitivity, improve model robustness, and enhance predictive accuracy, ensuring that variations in system inputs do not lead to misleading conclusions in process optimization and decision-making.

We calculate Pearson correlation coefficients between each reaction parameter (input variables) and biodiesel yield (output variable). The correlation values range from -1 to 1 and are represented in the bar diagram (Fig. 3). Fig. 3 illustrates that reaction parameters r_{1f}, r_{2f}, and M_c positively influence biodiesel production, whereas reaction parameters r_{1b} have a negative impact on biodiesel yield. This analysis helps identify the most significant factors that affect the efficiency of biodiesel production.

Fig. 4 presents the scatter plot corresponding to the partial rank correlation coefficients analysis (partial rank correlation coefficient), illustrating the relationship between reaction parameters and biodiesel production. In the plot, the X-axis represents the normalized values of each reaction parameter, while the Y-axis denotes the biodiesel yield. This visualization helps in understanding the strength and direction of the correlation between individual parameters and biodiesel production efficiency.

6.3 Numerical illustration

In the biodiesel production process, we employ the molar ratio of WCO-to-methanol, along with ultrasound, to investigate their respective effects.

Fig. 5 represents the concentration trajectories of triglyceride, methanol, diglyceride, monoglyceride, biodiesel, and glycerol utilizing 50 kHz ultrasound frequency and 5:1 methanol-to-WCO molar ratio using CF method of system (3.5) for fractional order

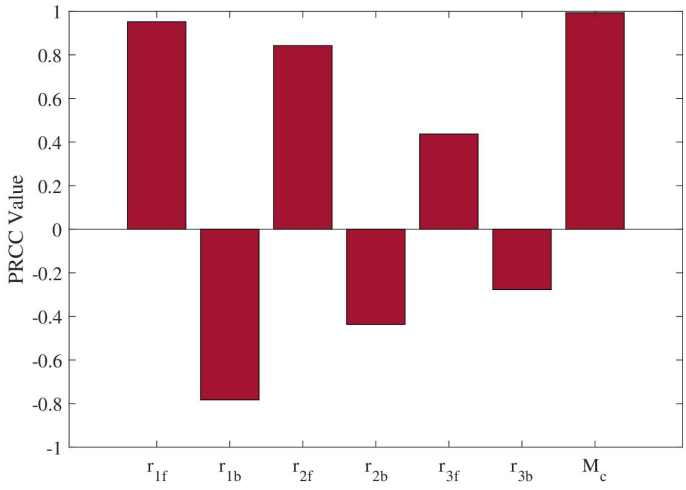

Figure 3: Bar diagram depicting the sensitivity of model parameters on biodiesel yield using integer order system, assessed through partial rank correlation coefficients using Pearson's correlation coefficient.

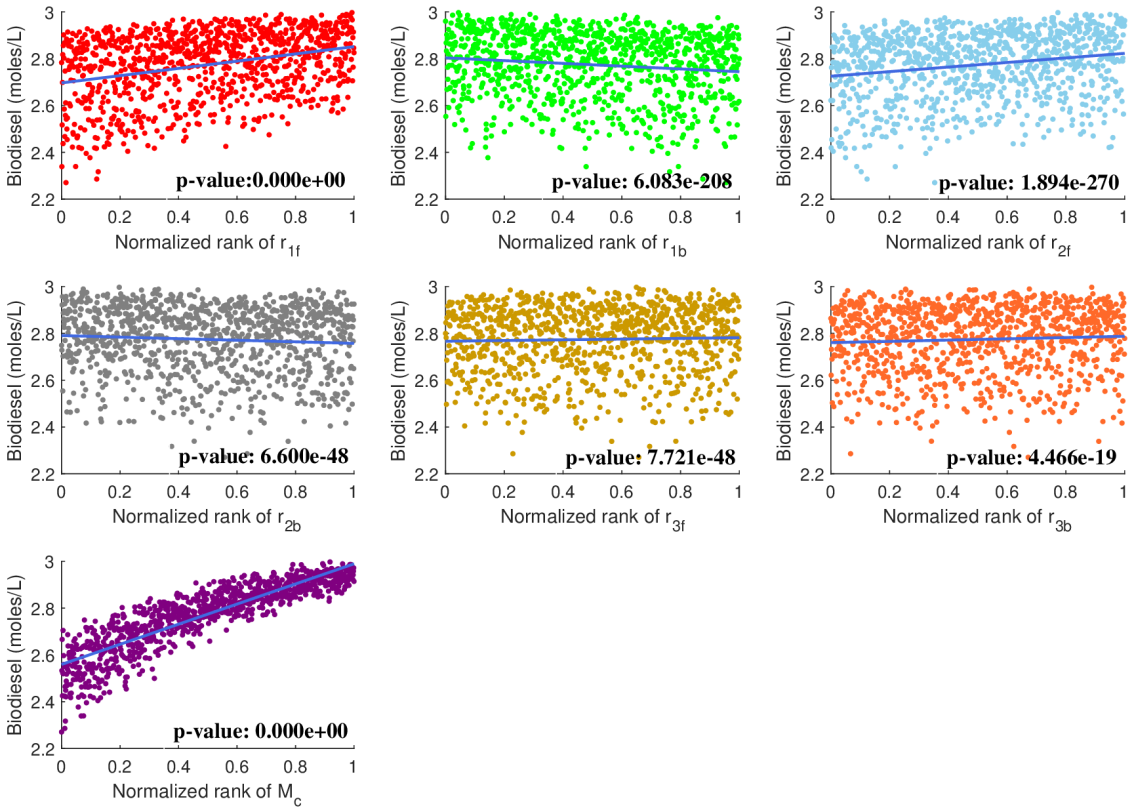

Figure 4: Scatter plot is presented for biodiesel production, illustrating the relationship between all reaction rates, including the mass transfer coefficient M_c. The statistical significance level is set at 0.05, meaning there is a 5% probability of rejecting a true null hypothesis. Each parameter is sampled $1{,}000$ times using the Latin hypercube sampling approach with a uniform probability distribution, ensuring comprehensive exploration of parameter space while maintaining statistical robustness.

$\phi = 0.85, 0.9, 0.95$ and 1 with reaction rate parameter $R = 0.3$. The trajectories highlight the influence of fractional-order derivatives on the reaction kinetics, where lower fractional orders ($\phi < 1$) introduce memory effects that slow down the depletion of reactants and the formation of products compared to the integer-order case ($\phi = 1$). This behavior is biologically significant as it suggests that transesterification exhibits a non-instantaneous response to reactant interactions. Fig. 6 shows the concentration trajectories of all the six reactants for the same ultrasound frequency and molar ratio with $\theta = 0.85, 0.9, 0.95$, and 1 with the same R-value as previous of ABC method. The observed variations in reactant concentration trends highlight the effectiveness of the non-singular kernel in capturing memory effects, which are absent in the integer-order model ($\theta = 1$).

Figs. 7 and 8 illustrate the impact of varying the memory rate parameter R on the chemical system using the CF and ABC fractional operators, with the fractional order fixed at 0.95 and memory rate values set at $R = 0.1, 0.3, 0.5, 0.7, 0.9$. Biologically, this variation in R reflects the extent to which past states of the reaction influence the present

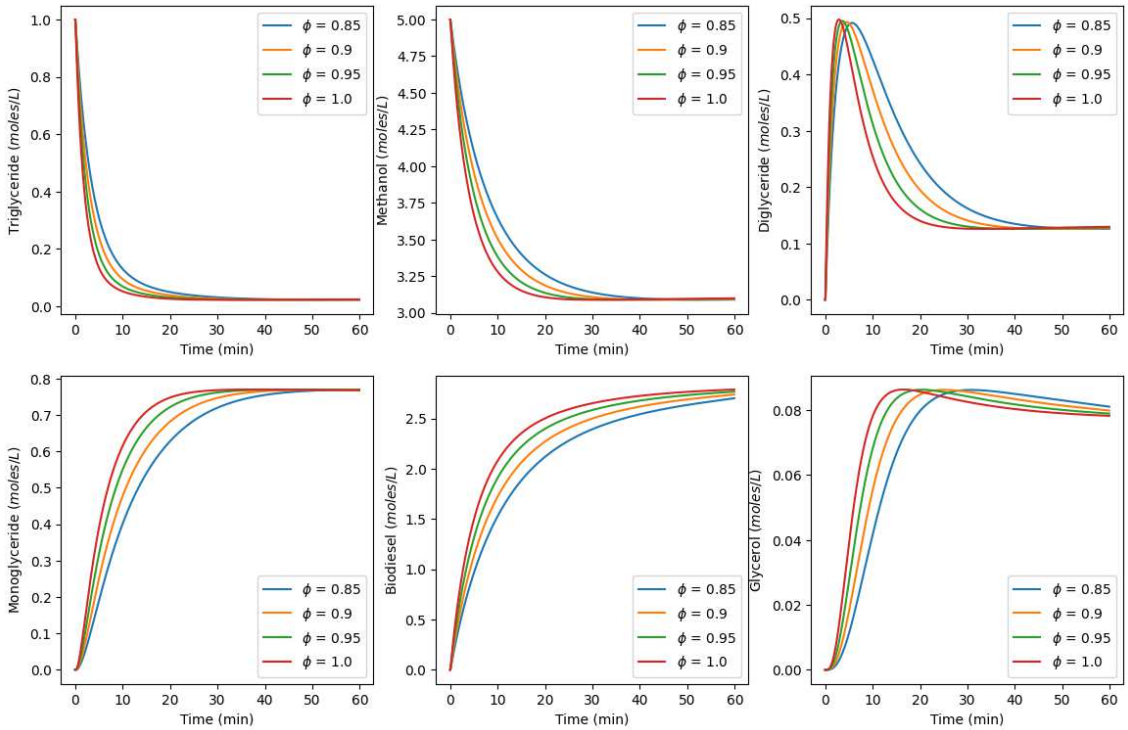

Figure 5: Concentration variation of all reactants over time in base-catalyzed transesterification using the CF method with fractional order $\phi = 0.85, 0.9, 0.95$, and 1. Memory rate parameter, $R = 0.3$, and other parameter values are specified in Tables 1 and 2. Here, the ultrasound frequency $H = 50\,\text{kHz}$, temperature $T = 50^{\circ}\text{C}$, and methanol-to-oil ratio is $5{:}1$.

biodiesel formation rate, which is crucial in complex biochemical and catalytic processes. A higher memory rate enhances the system's ability to retain past kinetic information, leading to a more sustained biodiesel yield, whereas lower values of R indicate a reaction dynamic that is more dependent on instantaneous conditions rather than historical effects.

The comparison between the CF and ABC methods in Fig. 9, with $\phi = \theta = 0.95$ and $R = 0.3$, reveals that biodiesel conversion from triglycerides (TG) is higher in the ABC method, as observed in subplots $(2,3,5)$. This difference arises due to the distinct kernel structures of the two fractional operators, where the ABC method, utilizing a Mittag-Leffler function, accounts for a broader and more persistent memory effect compared to the CF method's exponential kernel. The enhanced memory retention in the ABC model allows for a more sustained reaction rate, leading to greater biodiesel yield over time.

Figs. 10 and 11 represent the comparison through the surface plot for CF and ABC-induced systems with memory rate parameter value $R = 0.3$. In particular, Fig. 10(A) shows the surface plot of the biodiesel production with respect to the variation of fractional order "ϕ" and the molar ratio between methanol and WCO of the CF model (3.4). Fig. 10(B) represents the surface plots for biodiesel production with the variation of frac-

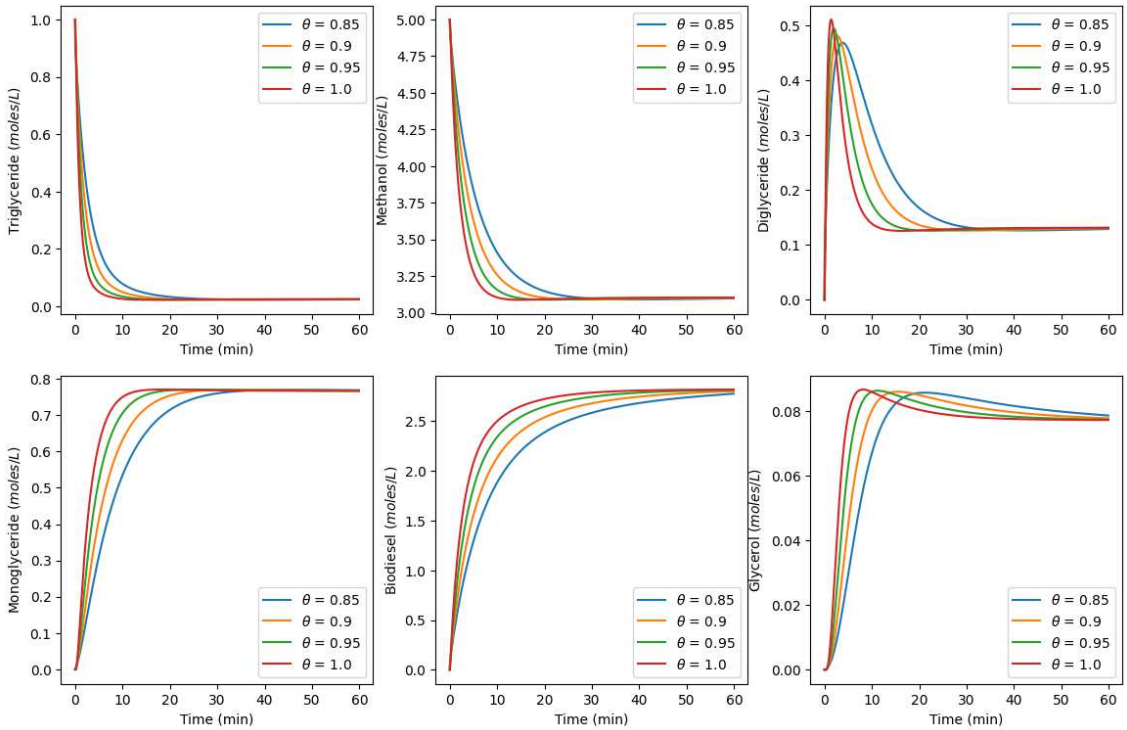

Figure 6: Variation of concentration of all the reactants over time in base-catalyzed transesterification using the ABC method with fractional order $\theta = 0.85, 0.9, 0.95$ and 1. Other parameter values are specified in Tables 1 and 2. Here, memory rate parameter $R = 0.3$, the ultrasound frequency $H = 50\text{kHz}$, temperature $T = 50^{\circ}C$, and methanol-to-oil ratio is $5:1$.

tional order "θ" and molar ratio using ABC method. Any coordinates on this surface represent the final molar conversion of biodiesel after 60 minutes for a particular molar ratio and fractional order. Similarly, Fig. 11(A) represents the surface plot for biodiesel production with the variation of applied ultrasound frequency "H" and fractional order "ϕ" in CF method and Fig. 11(B) represents the surface plots for biodiesel production with the variation of fractional order "θ" and ultrasound frequency for ABC method. In these cases, the range of fractional order ϕ or θ, molar ratio of methanol and WCO, and ultrasound frequency are from 0.8 to 1, $3:1$ to $6:1$, and 30 kHz to 60 kHz, respectively.

6.4 Experimental validity

To validate our simulated data over time, we compared it with experimental data from Takase [22] using both the ABC and CF methods. For this validation, 12 fractional order values θ or ϕ ranging from 0.7 to 1 were considered over a 120-minute period, utilizing 2400 iterations to ensure accuracy. From this range of fractional order, two values for ABC and two values of CF are chosen.

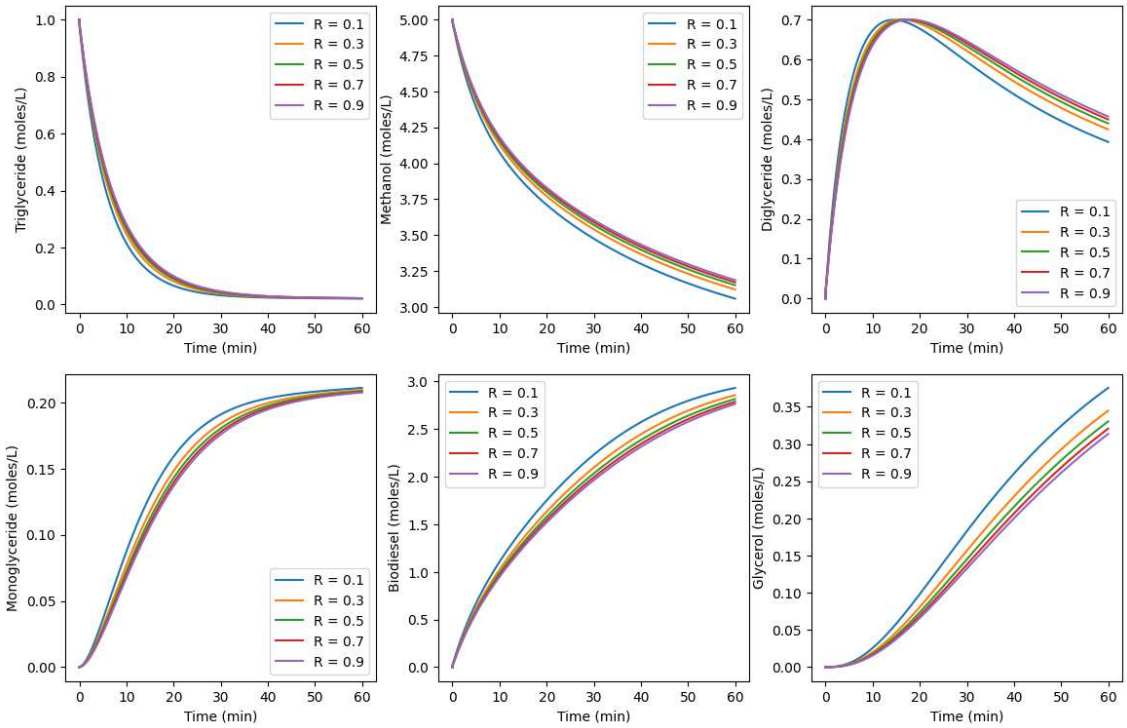

Figure 7: Time-dependent variation of concentration profiles for all reactants involved in the transesterification reaction using the CF fractional-order method with fractional order $\phi = 0.95$. The simulations are performed for five different values of the memory rate parameter $R = 0.1, 0.3, 0.5, 0.7$, and 0.9 to analyze its influence on reaction kinetics. All parameter values are taken as specified in Tables 1 and 2.

For ABC method: The bar diagram 12 compares biodiesel production between experimental data and the ABC fractional-order model at $\theta = 0.89$ and $\theta = 0.918$ over reaction times from 0 to 120 minutes. Initially (5-20 min), both ABC models and experimental data follow a similar increasing trend, though ABC ($\theta = 0.89$) slightly underestimates yield while ABC ($\theta = 0.918$) aligns more closely. At 10-15 min, both ABC models approximate experimental values well, though $\theta = 0.918$ slightly overestimates. At 20 minutes, both models predict a slightly higher yield than experimental data. In the mid-reaction phase (40-60 min), all datasets align closely, with minimal deviations at 40 min and near-identical values at 60 min, confirming the ABC model's accuracy in capturing biodiesel production rates. In the final phase (90-120 min), biodiesel production saturates, with all datasets converging at nearly the same values, demonstrating the ABC model's effectiveness in predicting steady-state production. The results indicate that while $\theta = 0.918$ provides a closer match at lower reaction times, both models perform well beyond 40 min, highlighting the fractional-order derivative's ability to capture memory effects and improve long-term predictions. The smooth convergence to experimental values suggests that the ABC fractional-order model effectively retains historical reaction dynamics, mak-

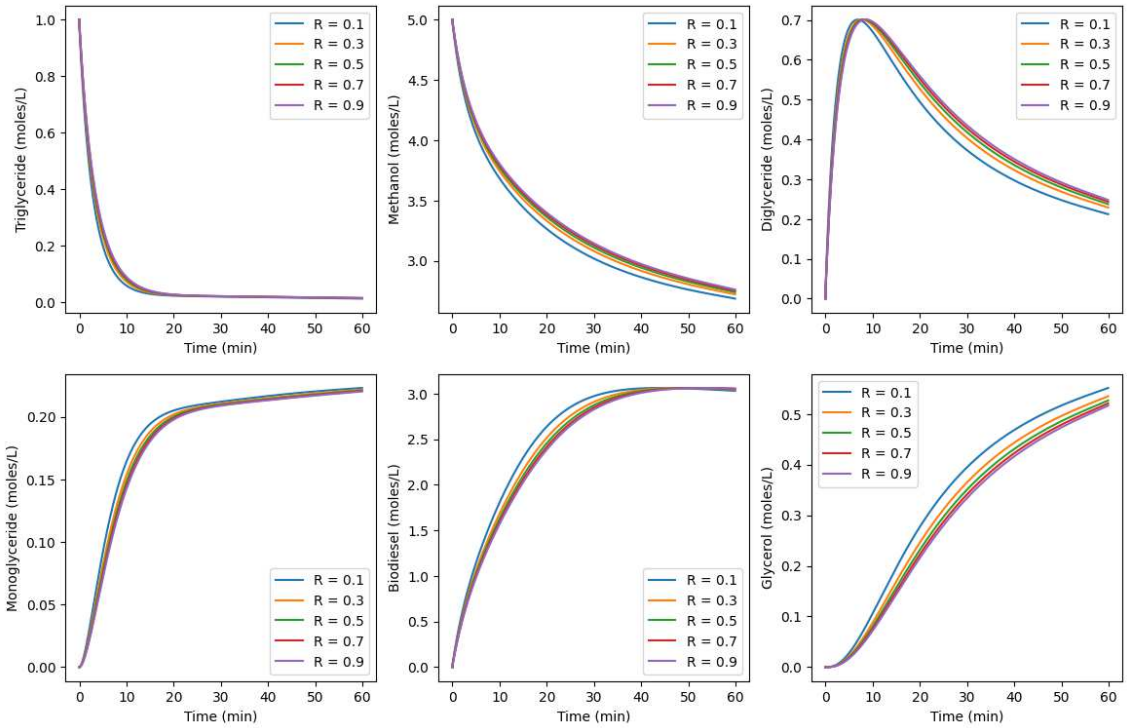

Figure 8: Variation of concentration profiles for all reactants involved in the transesterification reaction over time, modeled using the ABC fractional-order method with a fractional order of $\theta = 0.95$. R remains consistent with the values specified earlier. Model parameters are taken from Tables 1 and 2. These figures illustrate the dynamic behavior of reactants and products, highlighting the influence of fractional-order derivatives on reaction kinetics and memory effects in biodiesel production.

ing it a promising approach for biodiesel production modeling. Among the tested values, $\theta = 0.918$ offers the best overall fit, emphasizing the importance of optimizing fractional order for improved accuracy, with further experimental validation required to refine the model under different reaction conditions.

For CF method: The bar diagram (Fig. 13) compares biodiesel production using experimental data with the CF fractional-order model at two different values of fractional order: CF ($\phi = 0.97$) – blue bars, CF ($\phi = 1$) – gray bars, and experimental data – orange bars. In the early phase (5-20 min), the CF ($\phi = 0.97$) model slightly underestimates biodiesel yield at 5 min compared to experimental data, while CF ($\phi = 1$) is closer. At 10 min and 15 min, both CF models approach experimental values but still remain slightly lower. At 20 min, the CF ($\phi = 1$) model more accurately follows experimental data than CF ($\phi = 0.97$), which slightly underpredicts the yield. In the mid-reaction phase (40-60 min), both CF models align well with experimental values, with minimal deviation at 40 min. At 60 min, experimental and simulated results converge, indicating the CF method effectively captures reaction dynamics. In the final phase (90-120 min), all three datasets converge, confirming that both CF models accurately predict steady-state

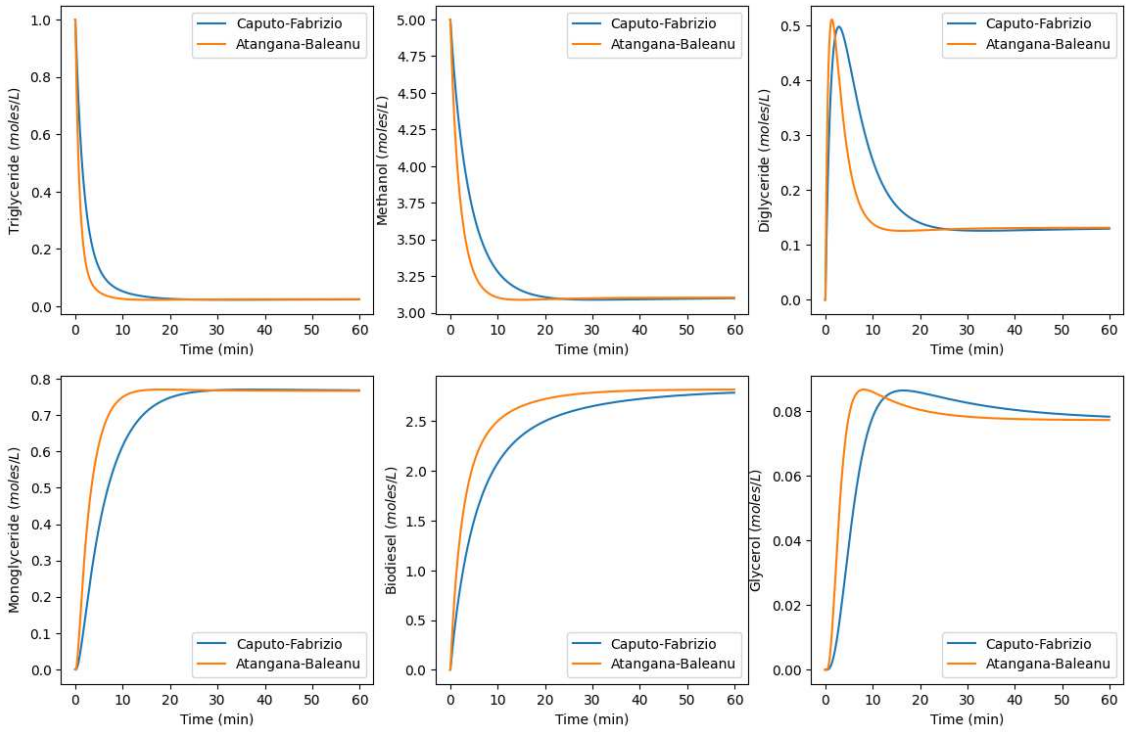

Figure 9: Comparison of the concentration profile of reactants in the transesterification reaction modeled with the CF and ABC fractional operators. With fractional orders $\phi = \theta = 0.95$ and $R = 0.3$, the figure highlights differences in reactant consumption and product formation, demonstrating how each fractional model captures the reaction dynamics.

biodiesel production. Overall, the CF fractional operator provides a better fit for integer order $\phi = 1$ across reaction times compared to fractional order $\phi = 0.97$, especially in the initial phase. The results suggest that the CF fractional-order model effectively retains reaction memory for the range 0.97 to 1, but precise tuning of ϕ is essential for improved accuracy.

Optimal control: To overcome the initial mass transfer resistance between methanol and WCO, ultrasound frequency is applied at the start of the reaction. Once the reaction gains momentum, ultrasound frequency is no longer required. To enhance cost-effectiveness, we can switch off the frequency at that stage. Fig. 14(a) shows the comparison of biodiesel production after employing optimal control technique on the ultrasound frequency for the ABC fractional method with using the best fitted fractional order $\theta = 0.918$ and Fig. 14(b) is the corresponding control profile. From the figure, it is evident that after 30 minutes we can switch off the ultrasound frequency. Fig. 14(a) demonstrates that by applying control on ultrasound frequency the production of biodiesel can be enhanced by 4-6% and also the process will be more cost-effective.

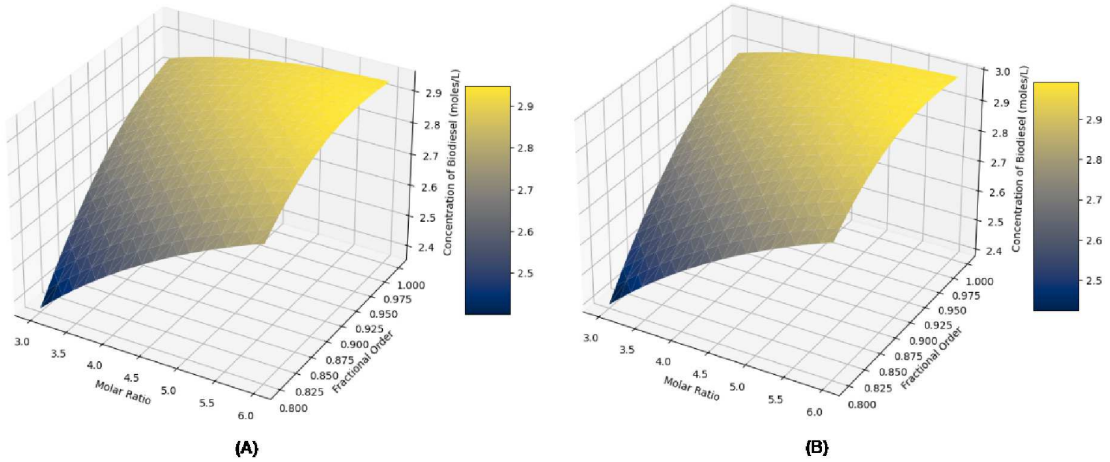

Figure 10: Surface plot for the concentration of biodiesel after 60 minutes with the variation of molar ratio of methanol and WCO from $3:1$ to $6:1$ and fractional order ϕ or θ from 0.8 to 1 using (A) CF and (B) ABC fractional operator. Here $H=50\text{kHz}$, $R=0.3$, and other parameter values taken from Tables 1 and 2.

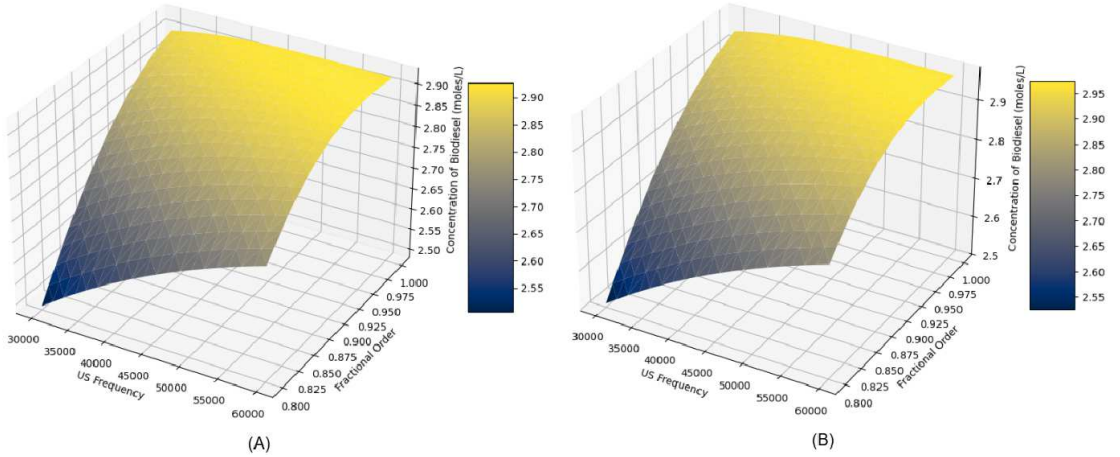

Figure 11: Surface plot for the concentration of biodiesel after 60 minutes with the variation of ultrasound frequency from 30kHz to 60kHz and fractional order ϕ or θ from 0.8 to 1 using (A) CF and (B) ABC fractional operator. Here the molar ratio of methanol and WCO is $5:1$, $R=0.3$, and other parameter values taken from Tables 1 and 2.

7 Discussion and conclusion

In this study, we have studied the transesterification reaction mechanism for biodiesel production from waste cooking oil (WCO) with fractional order derivative. We investigate the memory effect in the transesterification reaction of biodiesel using two distinct non-singular kernels: the exponential decay kernel and the Mittag-Leffler kernel. The whole study is conducted within a 1-meter of vessel diameter, at constant $50^{\circ}C$ tempera-

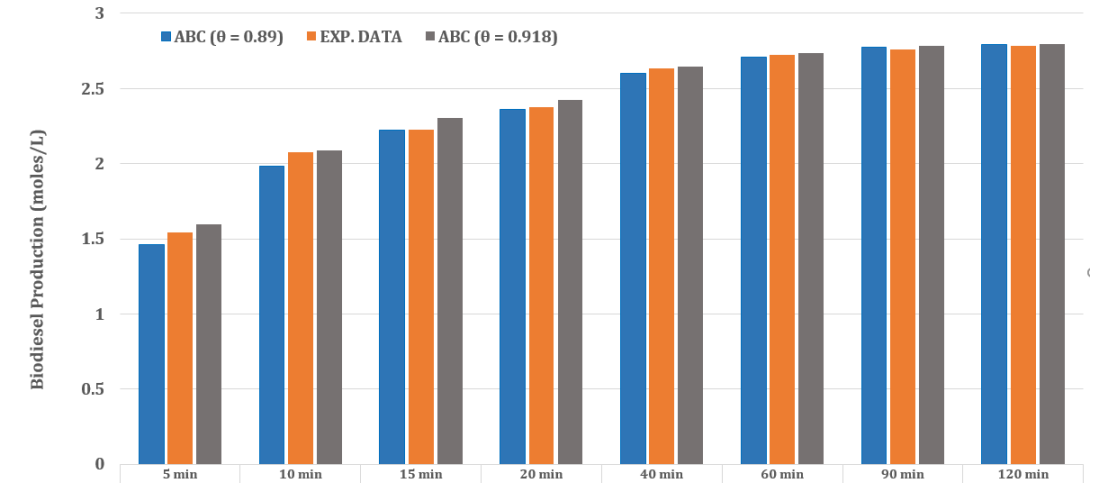

	5 min	10 min	15 min	20 min	40 min	60 min	90 min	120 min
ABC (θ = 0.89)	1.461548561	1.982742091	2.224139905	2.358969094	2.602056283	2.707717794	2.773065027	2.79367996
EXP. DATA	1.5407	2.0767	2.2273	2.3757	2.6353	2.7238	2.7585	2.7814
ABC (θ = 0.918)	1.594654506	2.090524879	2.304952388	2.424205793	2.64682081	2.73763681	2.785093068	2.797028893

Figure 12: Comparison of experimental data against simulated data for biodiesel production using ABC fractional operator with fractional order $\theta = 0.89$ and $\theta = 0.918$. Data in eight different times also been given in tabular form.

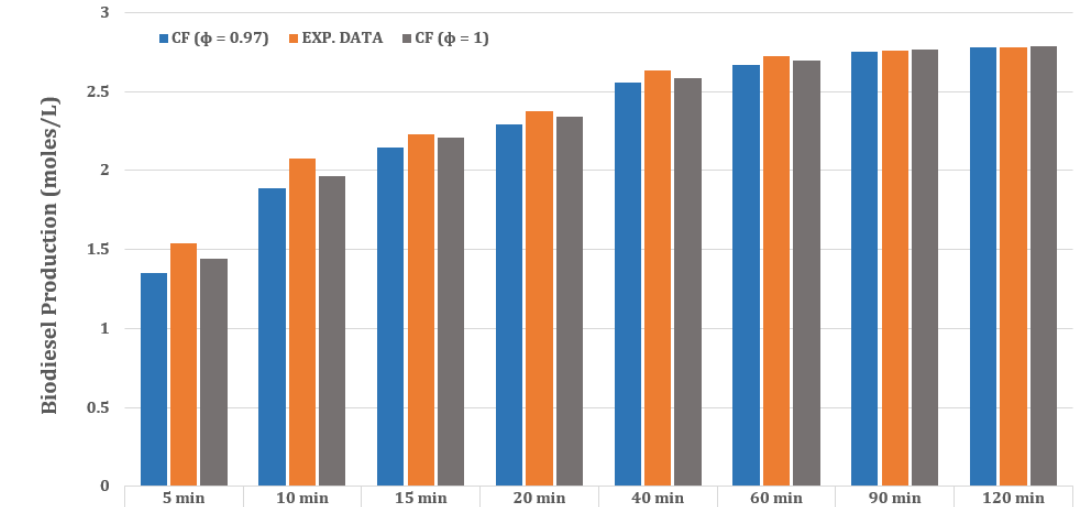

	5 min	10 min	15 min	20 min	40 min	60 min	90 min	120 min
CF (ϕ = 0.97)	1.348990157	1.887541987	2.147681099	2.294381283	2.553867775	2.669601176	2.751190679	2.782666012
EXP. DATA	1.5407	2.0767	2.2273	2.3757	2.6353	2.7238	2.7585	2.7814
CF (ϕ = 1)	1.439649041	1.966335114	2.208601687	2.343529909	2.587065218	2.694548894	2.764143982	2.787963737

Figure 13: Comparison of experimental data against simulated data for biodiesel production using CF fractional operator with fractional order $\phi = 0.97$ and $\phi = 1$. Data in eight different times also been given in tabular form.

ture, and 5:1 methanol to WCO molar ratio. Additionally, a 50kHz ultrasound frequency is applied to the system to enhance mixing and reduce the initial mass transfer resistance between oil and methanol.

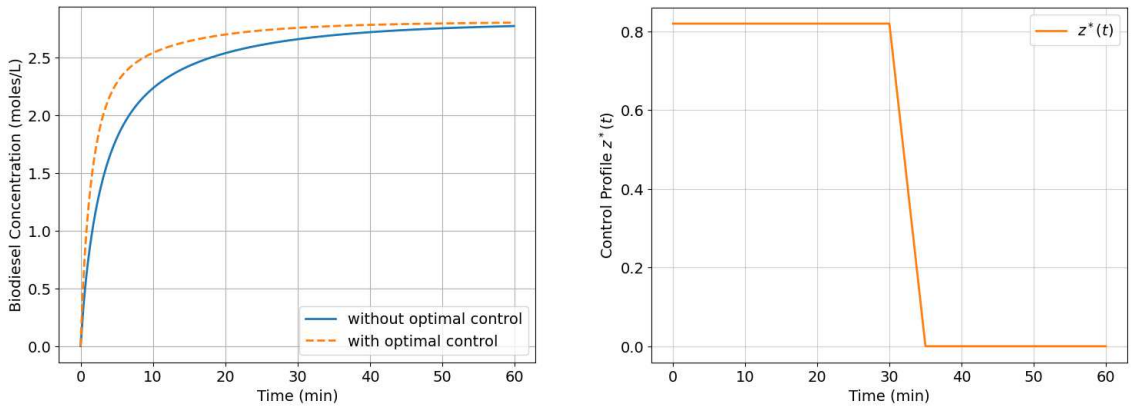

(a) (b)

Figure 14: (a) Comparison of the concentration profile of biodiesel after using optimal control technique for the ABC fractional method utilizing the best fitted fractional order $\theta=0.918$ and (b) is the corresponding optimal control profile. Here $H=50$kHz, methanol:WCO $=5:1$ and all the other parameter values taken from Tables 1 and 2.

In Sections 4.1 and 4.2, we analyzed the existence and uniqueness of the system (3.6) for the ABC fractional operator using the well-established Banach fixed-point theorem and the Arzelà-Ascoli theorem. Section 5 explores the formulation and solution of an optimal control problem for the model (3.6) using the ABC operator. By applying the Pontryagin minimum principle and Hamiltonian approach, we derived the optimal control profile $z^*(t)$. A comprehensive numerical scheme for both the CF and ABC operators is developed in Section 6.1. Using these numerical schemes, the solution of the systems (3.5) and (3.6) are graphically represented in Section 6.2.

In Figs. 5 and 6, the effect of memory on the reactants through the non-singular kernel is shown using both CF and ABC fractional operators for a fixed memory rate parameter's value, $R=0.3$ with the variation of fractional order ϕ and θ. In Figs. 7 and 8, the effect of memory rate parameter R is shown for both the fractional method for order $\phi=\theta=0.95$. In Fig. 9 comparison is made for fractional order 0.95 between two non-singular kernel methods. In Figs. 10 and 11 surface plots for final biodiesel production with respect to fractional order, the molar ratio of methanol and WCO, and ultrasound frequency are plotted for both the fractional method. In Section 6.4, detailed experimental validity is given for both CF and ABC systems and determines the order of the fractional derivatives. Additionally, the optimal control profile for maximum biodiesel production utilizing the best-fitted fractional order for the ABC fractional method and the corresponding improvements of production is plotted in Fig. 14.

In conclusion, the study confirms that the ABC fractional-order model ($\theta=0.918$) provides the best fit with experimental data, particularly in the early phase, due to its superior ability to retain memory effects. While the CF model aligns well at integer order ($\phi=1$), it lacks accuracy at fractional orders (i.e. for $0<\phi<1$). Both models converge with experimental data in later stages, demonstrating their reliability in biodiesel kinet-

ics modeling. Overall, the ABC model proves to be a more effective tool for capturing the history-dependent nature of transesterification reactions, making it a promising approach for optimizing biodiesel production. Finally, by controlling ultrasound frequency over time, biodiesel production can be increased by 4-6%.

This study has certain limitations. The comparison of biodiesel production using CF and ABC fractional models is based on a limited set of experimental data obtained under fixed reaction conditions, specifically at a constant temperature, molar ratio of alcohol to oil, catalyst concentration, and ultrasound frequency. However, biodiesel yield and reaction kinetics are highly sensitive to variations in these parameters. Changes in reaction temperature can alter the rate of transesterification and side reactions like saponification, while different molar ratios of alcohol to oil may influence reaction equilibrium and biodiesel conversion efficiency. Additionally, modifications in ultrasound frequency or mechanical stirring intensity can affect mass transfer rates and catalyst dispersion, leading to deviations in biodiesel yield compared to the results obtained in this study. To improve the applicability of fractional-order modeling, future research should systematically analyze these parameters and optimize reaction conditions to enhance model accuracy and practical implementation.

Acknowledgments

Priti Kumar Roy acknowledges the DST-FIST Programme, Government of India (No. SR/FST/MS II/2021/101(C)), Department of Mathematics, Jadavpur University, Kolkata-700032. Tushar Ghosh is supported by the UGC-JRF (NTA Ref. No. 211610107883), New Delhi, India.

References

[1] S. M. Ahammed, P. K. Roy, and S. Wang, *Effect of ultrasound technique for production of biodiesel using enzyme as catalyst: A mathematical study*, in: International Conference on Mathematical Analysis and Application in Modeling, Springer, 251–261, 2023.

[2] F. Al Basir, P. K. Roy, and S. Ray, *A fractional order mathematical model for enzymatic biodiesel synthesis and its optimization*, Int. J. Math. Models Methods Appl. Sci., 11:170–177, 2017.

[3] A. Atangana and D. Baleanu, *New fractional derivatives with nonlocal and non-singular kernel: Theory and application to heat transfer model*, arXiv:1602.03408, 2016.

[4] S. Banga et al., *Biodiesel production from waste cooking oil: A comprehensive review on the application of heterogeneous catalysts*, Energy Nexus, 10:100209, 2023.

[5] P. T. Benavides and U. Diwekar, *Optimal control of biodiesel production in a batch reactor: Part I: Deterministic control*, Fuel, 94:211–217, 2012.

[6] M. Berrios, M. Martín, A. Chica, and A. Martín, *Study of esterification and transesterification in biodiesel production from used frying oils in a closed system*, Chem. Eng. J., 160(2):473–479, 2010.

[7] X. Cao, S. M. Ahammed, S. Datta, J. Chowdhury, and P. K. Roy, *Enhancement of biodiesel production via ultrasound technology: A mathematical study*, ACS Omega, 9(18):20502–20511, 2024.

[8] M. Caputo, *Elasticità e Dissipazione*, Zanichelli, 1969.
[9] M. Caputo and M. Fabrizio, *A new definition of fractional derivative without singular kernel*, Prog. Fract. Differ. Appl., 1(2):73–85, 2015.
[10] G. K. Edessa, *Existence and uniqueness solution of the model of enzyme kinetics in the sense of Caputo-Fabrizio fractional derivative*, Int. J. Differ. Equ., 2022(1):1345919, 2022.
[11] W. H. Foo, W. Y. Chia, D. Y. Y. Tang, S. S. N. Koay, S. S. Lim, and K. W. Chew, *The conundrum of waste cooking oil: Transforming hazard into energy*, J. Hazard. Mater., 417:126129, 2021.
[12] B. Freedman, R. O. Butterfield, and E. H. Pryde, *Transesterification kinetics of soybean oil* 1, J. Am. Oil Chem. Soc., 63:1375–1380, 1986.
[13] K. Ganesan, K. Sukalingam, and B. Xu, *Impact of consumption of repeatedly heated cooking oils on the incidence of various cancers – a critical review*, Crit. Rev. Food Sci. Nutr., 59(3):488–505, 2019.
[14] A. Khan, K. Ali Abro, A. Tassaddiq, and I. Khan, *Atangana-Baleanu and Caputo-Fabrizio analysis of fractional derivatives for heat and mass transfer of second grade fluids over a vertical plate: A comparative study*, Entropy, 19(8):279, 2017.
[15] J. Lebl, *Basic Analysis I: Introduction to Real Analysis, Volume I*, 2018. `https://www.jirka.org/ra/`
[16] C. Lopresto, *Sustainable biodiesel production from waste cooking oils for energetically independent small communities: An overview*, Int. J. Environ. Sci. Technol., 22:1953–1974, 2025.
[17] S. Patnaik, J. P. Hollkamp, and F. Semperlotti, *Applications of variable-order fractional operators: A review*, Proc. R. Soc. Lond., Ser. A, Math. Phys. Eng. Sci., 476(2234):20190498, 2020.
[18] L. S. Pontryagin, *Mathematical Theory of Optimal Processes*, CRC Press, 1987.
[19] N. A. Sheikh, F. Ali, M. Saqib, I. Khan, S. A. A. Jan, A. S. Alshomrani, and M. S. Alghamdi, *Comparison and analysis of the Atangana-Baleanu and Caputo-Fabrizio fractional derivatives for generalized Casson fluid model with heat generation and chemical reaction*, Results Phys., 7:789–800, 2017.
[20] J. Singh, D. Kumar, and D. Baleanu, *On the analysis of chemical kinetics system pertaining to a fractional derivative with Mittag-Leffler type kernel*, Chaos, 27(10):103113, 2017.
[21] M. Suzihaque, H. Alwi, U. K. Ibrahim, S. Abdullah, and N. Haron, *Biodiesel production from waste cooking oil: A brief review*, Materials Today: Proceedings, 63:S490–S495, 2022.
[22] M. Takase, *Biodiesel yield and conversion percentage from waste frying oil using fish shell at Elmina as a heterogeneous catalyst and the kinetics of the reaction*, Int. J. Chem. Eng., 2022(1):8718638, 2022.
[23] V. V. Uchaikin, *Fractional Derivatives for Physicists and Engineers: Volume* 2, *Applications*, Springer, 2013.
[24] Y. Xu, W. Du, and D. Liu, *Study on the kinetics of enzymatic interesterification of triglycerides for biodiesel production with methyl acetate as the acyl acceptor*, J. Mol. Catal. - B Enzym., 32(5–6):241–245, 2005.
[25] Y. Zhou, *Basic Theory of Fractional Differential Equations*, World Scientific, 2023.